ACTIVE SHIELDING OF CYLINDRICAL TRANSMIT COILS FOR LOW-FIELD MAGNETIC RESONANCE IMAGING

by

Igor S. Kravchuk

Diploma in Physics, Moscow Institute of Physics and Technology, 1988

THESIS SUBMITTED IN PARTIAL FULFILLMENT

OF THE REQUIREMENTS FOR THE DEGREE OF

MASTER OF SCIENCE

IN THE DEPARTMENT

OF

PHYSICS

SIMON FRASER UNIVERSITY

Summer 2005

APPROVAL

Name:	Igor S. Kravchuk
Degree:	Master of Science
Title of Thesis:	Active Shielding of Cylindrical Transmit Coils for Low-Field Magnetic Resonance Imaging
Examining Committee:	Dr. H.D. Trottier, Professor (Chair)
	Dr. M.E. Hayden, Associate Professor, Senior Supervisor
	Dr. S.P. Watkins, Professor, Supervisor
	Dr. D. Broun, Assistant Professor, Supervisor
	Dr. K.L. Kavanagh, Professor, Examiner
Date Approved:	August 8, 2005

SIMON FRASER UNIVERSITY

Partial Copyright Licence

Abstract

Simple yet effective cylindrical transmit and receive coils for low frequency magnetic resonance imaging (MRI) can be fabricated from a sine-phi distribution of windings. This thesis introduces the novel concept of an actively-shielded transmit coil. This coil produces a uniform oscillating magnetic field (a "B_1 field") transverse to the bore of a cylindrical volume (the patient volume) yet at the same time produces very little magnetic field outside of this region. In practice, this allows one to minimize undesirable inductive coupling between the B_1 coil and the myriad of other coils (B_0, gradient, shim) that are needed to implement MRI. Exact analytical solutions are derived for active shielding of the elementary building blocks of typical B_1 coils. Specifically, solutions for a single straight wire, a complete current loop, and a sine-phi current distribution on the surface of an infinite cylinder are derived. Following this, the results of an experimental study examining the magnetic fields produced by actively shielded B_1 coils is presented. The concepts described in this thesis are expected to be useful for emerging applications in low field nuclear magnetic resonance and magnetic resonance imaging.

to my school teacher Vladimir Lvovich Konovalenko, from whom I learned to appreciate the beauty of physics

Acknowledgments

I would like to thank my supervisor Michael Hayden for his encouragement and continued support during this project as well as his help in editing and revising this thesis. For many helpful discussions, I also want to thank Christopher Bidinosti. I also want to thank my family for their patience, encouragement and love.

Contents

List of Tables

List of Figures

Chapter 1

Introduction

This thesis is concerned with the design of a new type of coil that is expected to be useful for magnetic resonance imaging in very low magnetic fields. Specifically, it is a coil that can be used to produce a uniform oscillating magnetic field transverse to the axis of a cylinder and at the same time produce very little field outside of this region. In the parlance of nuclear magnetic resonance it is a B_1 coil; that is, a coil that produces the oscillating magnetic field (the "B_1 field") that is used to manipulate nuclear spins. The novel feature of the particular coil described in this thesis is that it is the first B_1 coil known to incorporate active shielding. By design, the magnetic field produced by this coil is tailored to fall off rapidly as one moves away from the region of high field homogeneity. In effect what has been done is to bring together for the first time two principles in the design of coils that produce tailored magnetic fields. The first of these is the fact that a perfectly homogeneous magnetic field can be produced transverse to the axis of an infinite cylinder (or in fact an extrusion of any ellipsoid [1]) by imposing a surface current density that varies as $\sin(\varphi)$. This concept is illustrated in Fig. 1.1. The second is that the magnetic fields produced by a coil can in principle be perfectly shielded (i.e. forced to be identically zero) beyond some distance by the imposition of an appropriate current density outside of the region of primary interest. This concept is commonly used in the design of shielded superconducting magnets and gradient coils for magnetic resonance imaging.

The reminder of this chapter sets the stage for the thesis. First, a brief introduction to low field magnetic resonance is given to motivate the need for the coil described in this thesis. This is followed by a brief discussion of the design of coils that incorporate

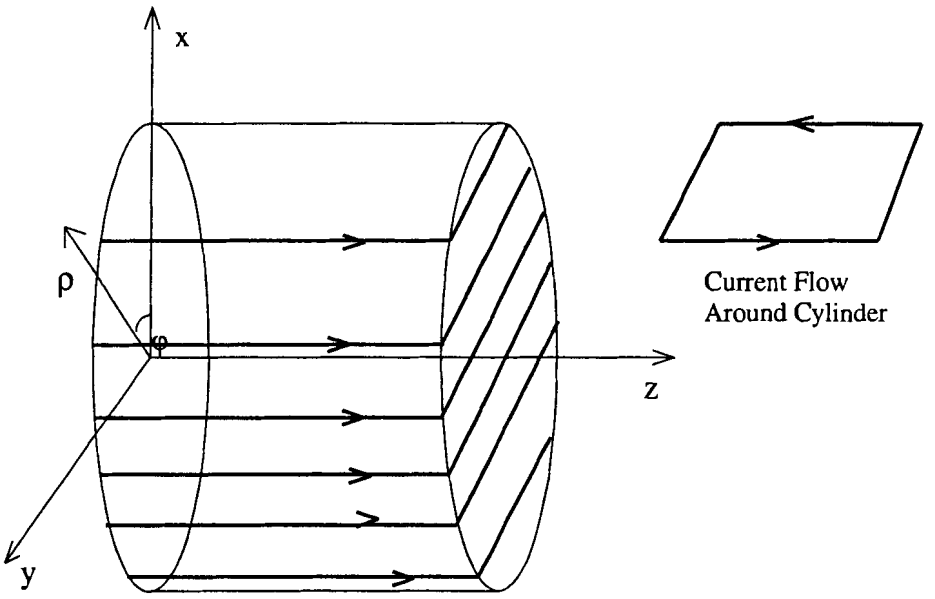

Figure 1.1: Approximation of a sine-phi current distribution by a network of loops.

active shielding. Several of the key theoretical concepts introduced in this thesis can be found in the article "Active Shielding of Cylindrical Saddle-shaped Coils: Application to Wire-wound RF Coils for Very Low Field NMR and MRI" by Christopher Bidinosti, Igor Kravchuk and Michael Hayden. At the time of writing, this article has been accepted for publication in the *Journal of Magnetic Resonance* [2]. Some of the experimental results presented in this thesis appear in the *Proceedings of the 12th Meeting of the International Society for Magnetic Resonance in Medicine.*

1.1 Magnetic resonance imaging

Nuclear magnetic resonance (NMR) and magnetic resonance imaging (MRI) are powerful diagnostic tools with numerous scientific applications, medical imaging being perhaps the most important. They make it possible to visualize a wide variety of tissue characteristics and to monitor biological functions. In recent years, there have been significant advances in the development of practical *gas phase* MRI, particularly for investigation of gas-filled lung tissue. In effect this field started in 1994 when, using ^{129}Xe gas polarized far beyond thermal equilibrium, a group of researchers from Princeton University were able to acquire an image of the gas-filled lungs of a mouse [3]. Since that time, a host of similar techniques have been used to image human lungs *in vivo*, promising the potential development of many new diagnostic applications.

Conventional MRI requires a large static magnetic field B_0 in order to polarize a collection of nuclear spins. In thermal equilibrium at temperature T the number of spins oriented parallel and antiparallel to the B_0 field (N_{up} and N_{down}) are related to one another via a Boltzmann factor

$$N_{up} = N_{down} \exp \frac{2\mu B_0}{kT} \tag{1.1}$$

where μ is the nuclear magnetic moment and k is Boltzmann's constant. At room temperature, the ensemble nuclear polarization for a spin $\frac{1}{2}$ system

$$P = \frac{N_{up} - N_{down}}{N_{up} + N_{down}} = \tanh\left(\frac{\mu B_0}{kT}\right) \tag{1.2}$$

is very small even in large magnetic fields $\vec{B}$. For example, in a typical medical MRI apparatus operating at $B = 1.5$ T, the polarization of H atoms is $P_H = 5$ ppm. However, NMR and MRI signal amplitudes depend on the total nuclear magnetization of a sample. The more nuclei that are present in a given sample, the easier it is to detect a signal. The concentration of H nuclei associated with water molecules in living tissue is about 100 moles/l. The corresponding polarization density clearly gives rise to signals that are readily detected with good signal-to-noise ratio.

The situation for pulmonary imaging is different. Because of the lung's low tissue density (which leads to a reduced signal intensity) and because of field gradients induced

by magnetic susceptibility differences between gas and tissue (which limits resolution and causes distortion), the lungs are perhaps the most difficult organ to image. Moreover, if one tries to imagine acquiring an image of thermally polarized gas inside the lungs, the situation is challenging [11, 12]. The concentration of nuclei in an atomic gas at room temperature and atmospheric pressure is 0.04 molar, a factor of 2,500 less than the concentration of protons in living tissue. The corresponding thermal equilibrium polarization density at 1.5 T is too low to be easily detected using conventional MRI techniques.

Gases with nuclear polarization far in excess of thermal equilibrium values can be prepared using optical pumping methods. These techniques, which involve transferring the spin angular momentum of circularly polarized light to the nuclei of atoms like ^{3}He or ^{129}Xe, were developed by A. Kastler during the 1950's (1966 Nobel Prize in Physics). In effect, these methods enable one to enhance the nuclear polarization of certain noble gases by many orders-of-magnitude without the need for an intense magnetic field. For example, nuclear polarizations as high as 85% have been obtained for ^{3}He at room temperature. The result of optical pumping is a highly non-equilibrium yet (in the right environment) long-lived nuclear polarization. As a consequence, fewer gas atoms are required to produce the same NMR or MRI signal response. For example, the polarization density of a gas of 50% polarized ^{3}He at room temperature and atmospheric pressure is about one hundred times greater than the polarization density of protons in living tissue in a 1.5 T magnetic field.

A direct consequence of using optically-polarized gases in MRI experiments is that a large static magnetic field is not required. All that is needed is a clearly defined quantization axis. Typically this can be achieved using a ~ 2 mT field for polarized gas MRI (as opposed to 1-3 Tesla for conventional high-field MRI). In turn, the Larmor frequency of the gas atoms ends up being extraordinarily low by conventional MRI standards, perhaps 100 kHz as opposed to many tens of Mhz. At first glance this would appear to be of enormous benefit as coil/resonator designs are much simpler in the quasistatic limit (dimensions $<<$ wavelength).

One complication that does arise, however is that it becomes difficult to use conventional passive shielding techniques to isolate a B_1 coil from the myriad of gradient and shim coils that one needs to implement MRI. Ordinarily a B_1 coil/resonator operating at 100 MHz in an MRI system is surrounded by a thin Faraday shield. The thickness and geometry of this shield are chosen so that it effectively shields the B_1 field at the Larmor

frequency but at the same time is almost transparent to gradient fields that might be switched at frequencies as high as a few tens of kHz. This natural separation of frequency scales is no longer an option when one considers low frequency MRI. The Larmor frequency of precessing nuclear spins can very easily end up being comparable to (or lower than!) the characteristic switching frequencies of gradient fields. Clearly, an alternate approach to the design of shielded B_1 coils suitable for this low field, low frequency regime is required.

1.2 Active shielding of coils

Passive shielding of RF coils is widely used in high-frequency NMR and MRI applications where a conducting cylinder of sufficient thickness will support the induced surface current (*i.e.* eddy current [5]) flow needed to contain B_1 fields. It becomes problematic in low-field, low-frequency NMR and MRI if the necessary thickness of the passive shield increases beyond a few millimeters. For example, in the kHz frequency range, a passive shield made of aluminum needs to be about $d \approx 10$ mm thick [9] if one requires $d >> \delta$, where δ is the skin depth of the metal[1]. Low-field, low-frequency NMR and MRI thus require new approaches to the design of shields for B_1 coils.

The problem of shielding the magnetic field produced by low-frequency coils generally requires the use of active rather than passive shields [8, 9]. This approach has been applied widely to the design of gradient coils [10, 6], but not previously to B_1 coils.

The design of an active shield is determined from a knowledge of the current that would be induced on a thick conducting surface placed at the location of the desired shield. This current is in turn linked to the current configuration of the RF coil via its magnetic field [9]. In other words, once the magnetic field B_1 is known on the surface of the shield, a surface current density $\vec{F}(\varphi, z)$ can be calculated from the boundary condition

$$\vec{B}_2 - \vec{B}_1 = \mu_0 \vec{F}(\varphi, z) \times \vec{n} \tag{1.3}$$

where $\vec{B}_1$ ($\vec{B}_2$) is the magnetic field on the inside (outside) of the surface, and $\vec{n}$ is a unit

[1] While $d >> \delta$ is often quoted as a necessary condition for effective shielding (particularly in elementary textbooks on Electricity and Magnetism), it is not a general requirement. Much thinner shields can be constructed. The interested reader should consult reference [7].

vector normal to the surface. Normally one is interested in having $\vec{B}_2 = 0$ for effective shielding. Knowing the surface current density $\vec{F}(\varphi, z)$ that is necessary for $\vec{B}_2 = 0$, the problem becomes one of trying to produce a reasonable approximation to it so that $\vec{B}_2$ is sufficiently small.

A common form of B_1 coil is a saddle-shaped coil. The magnetic fields produced by such (unshielded) coils have been studied previously by many authors [13, 14, 15, 16, 17, 18, 19, 20, 21]. Using any of these results, an appropriate shielding current density could be calculated using Eq. 1.3.

The approach used in this thesis follows the somewhat more advanced and general methods introduced by Turner and Bowley in an article entitled "Passive Screening of Switched Magnetic Field Gradients" [9]. Their method of analysis leads to exact and general relationships for shield surface currents in terms of coil parameters, which can in turn be used to design actively driven shields. Their discussion was restricted to problems involving current distributions on the surface of concentric cylinders, although in principle it could be generalized to concentric ellipses. The present discussion is likewise restricted to concentric cylinders as in many situations this tends to be a more practical geometry for coil construction.

1.3 Outline of thesis

The reminder of this thesis is structured as follows. In chapter 2 the main theoretical concepts underlying active shielding of coils are outlined. The approach is similar to the methodology introduced by Turner and Bowley [9] for the design of shielded gradient coils. These methods are successively applied to the elementary building blocks of low field B_1 coils. Specifically, analytic solutions are derived for the current distributions required to perfectly shield a single straight wire, a complete current loop, and a sine-phi current distribution on the surface of an infinite cylinder. Discrete approximations to these current distribution based on a finite number of current-carrying wires are also presented. In chapters 3 and 4 the design of a prototype shielded B_1 coil is described and a series of measurements characterizing its performance are summarized. Finally, chapter 5 summarizes the work described in this thesis and discusses avenues for future exploration.

Chapter 2

Theory: active shielding

In order to eliminate the undesired influence of magnetic fields produced by induced currents flowing in conducting structures located in the vicinity of RF coils, one needs to reduce the magnetic field produced by the coil to zero beyond some finite radius. A systematic theoretical approach to this problem was developed by R. Turner and R. M. Bowley [9] in the context of shielding the magnetic fields produced by gradient coils for MRI applications. Their work is described in the first part of this chapter. The remainder of the chapter is devoted to examples and extensions of Turner and Bowley's ideas that ultimately lead to the design of an actively-shielded cylindrical coil for $\vec{B}_1$ field generation.

2.1 R. Turner and R. M. Bowley's analysis

Turner and Bowley [9] begin their analysis by assuming that all currents flow on the surfaces of two coaxial cylinders of radii $\rho = a$ and $\rho = b$, where $a < b$. It is thus natural to use cylindrical coordinates that reflect the symmetry of the system. The z axis is taken to lie along the axis of the cylinders as shown in Fig. 2.1.

With the assumptions that the current on the inner cylinder ($\rho = a$) and the current induced in the shield ($\rho = b$) are confined to their surfaces, the radial part of the current density can be represented by a Dirac δ-function. That is, the general expression for currents can be written as

$$\vec{J} = \vec{F}(z,\varphi)\delta(\rho - a) + \vec{f}(z,\varphi)\delta(\rho - b) \tag{2.1}$$

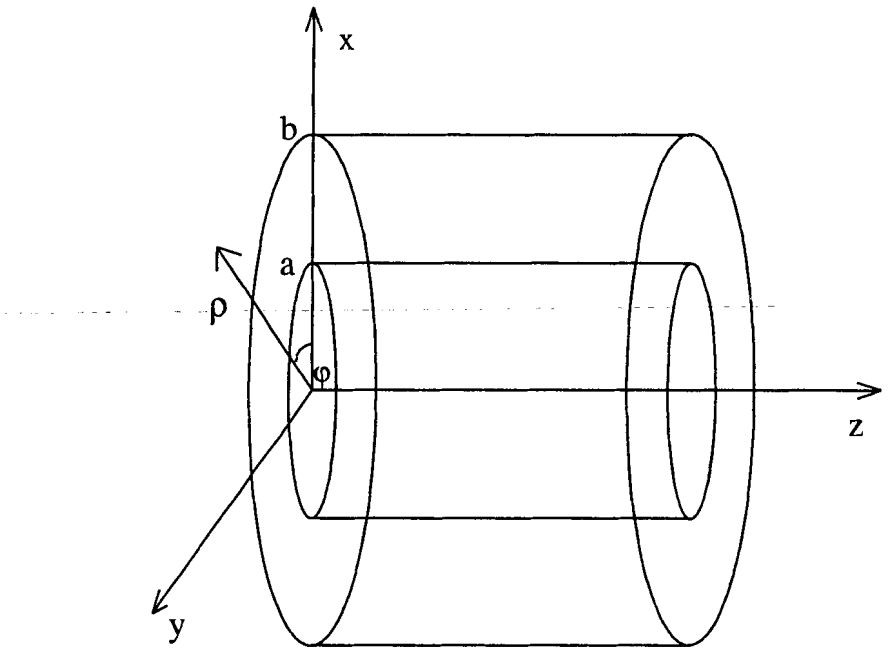

Figure 2.1: Coordinate system and surfaces on which currents are constrained to flow.

where $\vec{F}$ describes the surface current density on the inner cylinder and $\vec{f}$ describes the surface current density on the outer cylinder.

The magnetic field produced by these currents can be written in terms of the vector potential $\vec{A}$, which in cylindrical coordinates has components A_ρ, A_φ and A_z given by:

$$A_\rho = \frac{\mu_0}{4\pi}\int \frac{J_{\varphi'}(\vec{r}')dv'\sin(\phi-\phi')}{|\vec{r}-\vec{r}'|} \tag{2.2}$$

$$A_\varphi = \frac{\mu_0}{4\pi}\int \frac{J_{\varphi'}(\vec{r}')dv'\cos(\phi-\phi')}{|\vec{r}-\vec{r}'|} \tag{2.3}$$

$$A_z = \frac{\mu_0}{4\pi}\int \frac{J_z(\vec{r}')dv'}{|\vec{r}-\vec{r}'|} \tag{2.4}$$

where $\vec{J}$ only has z and φ components and must satisfy the continuity equation

$$\nabla\cdot\vec{J} = 0\,. \tag{2.5}$$

A further constraint, associated with the goal of eliminating the magnetic field for $\rho \geq b$, is that the radial component of the magnetic field should be zero on the surface of the outer cylinder:

$$B_\rho = 0\,. \tag{2.6}$$

The crux of Turner and Bowley's approach to the analytic treatment of these equations lies in a sequence of three steps. First, they introduce a Green's function expansion for the factor $\frac{1}{|\vec{r}-\vec{r'}|}$ appearing in Eqs. 2.2 through 2.4. Next, they identify terms in this expansion with Fourier transformations of the currents $\vec{F}(z,\varphi)$ and $\vec{f}(z,\varphi)$ appearing in Eq. 2.1. Finally, using the constraints Eqs. 2.5 and 2.6 they establish expressions for the Fourier transforms of the current density on the outer cylinder that completely eliminate the magnetic field beyond the outer cylinder ($\rho \geq b$). These steps are illustrated below.

The Green's function expansion of $\frac{1}{|\vec{r}-\vec{r'}|}$ in cylindrical coordinates (see for example the textbook by J.D.Jackson [22]) is:

$$\frac{1}{|\vec{r}-\vec{r'}|} = \frac{1}{\pi}\sum_{m=-\infty}^{\infty}\int_{-\infty}^{\infty} dk \exp[im(\varphi-\varphi')]\exp[ik(z-z')]I_m(k\rho^<)K_m(k\rho^>) \tag{2.7}$$

where $\rho^<(\rho^>)$ denotes the lesser (greater) of ρ and ρ', and $I_m(z)$ and $K_m(z)$ are modified Bessel functions of the first and second kind, respectively. The Fourier transformed currents on the inner and outer cylinders are:

$$f_z^m(k) = \frac{1}{2\pi}\int_{-\pi}^{\pi} d\varphi \exp(-im\varphi)\int_{-\infty}^{\infty} dz \exp(-ikz) f_z(\varphi,z) \tag{2.8}$$

$$f_\varphi^m(k) = \frac{1}{2\pi}\int_{-\pi}^{\pi} d\varphi \exp(-im\varphi)\int_{-\infty}^{\infty} dz \exp(-ikz) f_\varphi(\varphi,z) \tag{2.9}$$

$$F_z^m(k) = \frac{1}{2\pi}\int_{-\pi}^{\pi} d\varphi \exp(-im\varphi)\int_{-\infty}^{\infty} dz \exp(-ikz) F_z(\varphi,z) \tag{2.10}$$

$$F_\varphi^m(k) = \frac{1}{2\pi}\int_{-\pi}^{\pi} d\varphi \exp(-im\varphi)\int_{-\infty}^{\infty} dz \exp(-ikz) F_\varphi(\varphi,z) \tag{2.11}$$

where f_z^m, f_φ^m, F_z^m and F_φ^m are the components of $\vec{f}$ and $\vec{F}$. The components of $\vec{A}$ for $\rho > b$ are thus:

$$\begin{aligned} A_\varphi = \frac{\mu_o}{4\pi}\sum_{m=-\infty}^{\infty}\int_{-\infty}^{\infty} dk \exp(im\varphi)\exp(ikz)[b f_\varphi^m(k)(I_{m-1}(kb)K_{m-1}(k\rho) \\ + I_{m+1}(kb)K_{m+1}(k\rho)) + a F_\varphi^m(k)(I_{m-1}(ka)K_{m-1}(k\rho) \\ + I_{m+1}(ka)K_{m+1}(k\rho))] \end{aligned} \tag{2.12}$$

$$A_\rho = \frac{-i\mu_o}{4\pi}\sum_{m=-\infty}^{\infty}\int_{-\infty}^{\infty} dk \exp(im\varphi)\exp(ikz)[bf_\varphi^m(k)(I_{m-1}(kb)K_{m-1}(k\rho) - I_{m+1}(kb)K_{m+1}(k\rho)) + aF_\varphi^m(k)(I_{m-1}(ka)K_{m-1}(k\rho) - I_{m+1}(ka)K_{m+1}(k\rho))] . \quad (2.13)$$

$$A_z = \frac{\mu_o}{2\pi}\sum_{m=-\infty}^{\infty}\int_{-\infty}^{\infty} dk \exp(im\varphi)\exp(ikz)K_m(k\rho)\left[bI_m(kb)f_z^m(k) + aI_m(ka)F_z^m(k)\right] \quad (2.14)$$

The boundary condition that $B_\rho = 0$ at $\rho = b$ implies:

$$\frac{1}{b}\frac{\partial A_z}{\partial \varphi}\bigg|_{\rho=b} = \frac{\partial A_\varphi}{\partial z}\bigg|_{\rho=b} \quad (2.15)$$

and thus, when Eqs. 2.14 and 2.12 are substituted into Eq. 2.15 one obtains:

$$\frac{2m}{bk}K_m(kb)\left[bI_m(kb)f_z^m(k) + aI_m(ka)F_z^m(k)\right] = f_\varphi^m(k)b\left[I_{m-1}(kb)K_{m-1}(kb) + I_{m+1}(kb)K_{m+1}(kb)\right] + F_\varphi^m(k)a\left[I_{m-1}(ka)K_{m-1}(kb) + I_{m+1}(ka)K_{m+1}(kb)\right] . \quad (2.16)$$

This equation can be simplified using the requirement that currents must be continuous. In cylindrical coordinates this implies:

$$\frac{1}{b}\frac{\partial f_\varphi}{\partial \varphi} = -\frac{\partial f_z}{\partial z} \quad (2.17)$$

and

$$\frac{1}{b}\frac{\partial F_\varphi}{\partial \varphi} = -\frac{\partial F_z}{\partial z} . \quad (2.18)$$

Consequently, the Fourier transformed currents must satisfy:

$$f_\varphi^m(k) = -\frac{kb}{m}f_z^m(k) \quad (2.19)$$

and

$$F_\varphi^m(k) = -\frac{ka}{m}F_z^m(k) . \quad (2.20)$$

Equation 2.16 can be simplified using the identity

$$I_{m-1}(z_1)K_{m-1}(z_2) + I_{m+1}(z_1)K_{m+1}(z_2) + \left(\frac{2m^2}{z_1 z_2}\right)I_m(z_1)K_m(z_2) = -2I_m'(z_1)K_m'(z_2) \quad (2.21)$$

which can be derived using the recurrence relations for Bessel functions (see for example the book by M. Abramowitz and I.A. Stegun [23]). Finally, by combining expressions 2.16 through 2.21 Turner and Bowley obtained the following elegant expressions relating the Fourier transformed current densities on the inner and outer cylinders respectively:

$$f_z^m(k) = -F_z^m(k)\frac{a^2 I_m'(ka)}{b^2 I_m'(kb)} \tag{2.22}$$

and

$$f_\varphi^m(k) = -F_\varphi^m(k)\frac{a I_m'(ka)}{b I_m'(kb)} \; . \tag{2.23}$$

That is, given an arbitrary current density on the inner cylinder ($\rho = a$), Eqs. 2.22 and 2.23 enable one to calculate the current density on the outer cylinder ($\rho = b$) that is needed to completely eliminate the magnetic field for $\rho > b$. The use of these remarkable expressions is illustrated in the following sections.

2.2 Complete current loop

As a simple example, consider a current I flowing in the azimuthal direction and constrained to a loop of radius $\rho = a$ centered at $z = z_1$, as shown in Fig. 2.2. In the notation of the previous section this implies:

$$F_z = 0 \tag{2.24}$$

and

$$F_\varphi = I\delta(z - z_1) \; . \tag{2.25}$$

Making use of Eq. 2.11, we find:

$$\begin{aligned} F_\varphi^m &= \frac{I}{2\pi}\int_{-\pi}^{\pi} d\varphi \exp(-im\varphi)\int_{-\infty}^{\infty} dz \exp(-ikz) I\delta(z - z_1) \\ &= I\exp(-ikz_1)\delta_{m,0} \end{aligned} \tag{2.26}$$

and therefore

$$f_\varphi^m(k) = -I\frac{a}{b}\frac{I_m'(ka)}{I_m'(kb)}\exp(-ikz_1)\delta_{m,0} \tag{2.27}$$

which gives

$$f_\varphi^m(k) = -I\frac{a}{b}\frac{I_0'(ka)}{I_0'(kb)}\exp(-ikz_1) \; . \tag{2.28}$$

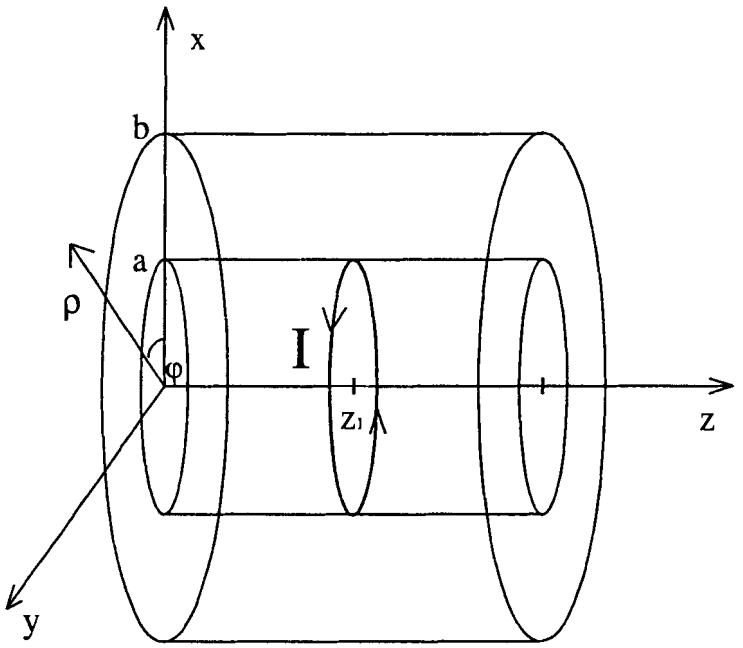

Figure 2.2: Current loop of radius $\rho = a$ centered at $z = z_1$.

The inverse Fourier transform of Eq. 2.28 gives the shielding current $f_\varphi(z)$ on $\rho = b$ required to eliminate $\vec{B}$ for $\rho > b$:

$$\begin{aligned} f_\varphi(z) &= -I\frac{a}{2\pi b}\int_{-\infty}^{\infty} dk \exp[ik(z-z_1)]\frac{I_0'(ka)}{I_0'(kb)} \\ &= -I\frac{a}{2\pi b}\int_{-\infty}^{\infty} dk \exp[ik(z-z_1)]\frac{I_1(ka)}{I_1(kb)} \\ &= -I\frac{a}{\pi b}\int_{0}^{\infty} dk \cos[k(z-z_1)]\frac{I_1(ka)}{I_1(kb)}\,, \end{aligned} \tag{2.29}$$

a result that has not previously been reported.

Note here that, once we know the shielding current density $f_\varphi(z)$, the total current flowing on the outer cylinder can be obtained:

$$\begin{aligned} I_s &= \int_{-\infty}^{\infty} f_\varphi(z)dz \\ &= -I\frac{a}{b}\int_{-\infty}^{\infty} dk \frac{I_0'(ka)}{I_0'(kb)}\left(\frac{1}{2\pi}\int_{-\infty}^{\infty} \exp ik(z-z_1)dz\right) \\ &= -I\frac{a}{b}\int_{-\infty}^{\infty} dk \frac{I_0'(ka)}{I_0'(kb)}\delta(k) \\ &= -I\frac{aI_0'(ka)}{bI_0'(kb)}\bigg|_{k=0} . \end{aligned} \tag{2.30}$$

Evaluation of the limit in Eq. 2.30 (see Appendix A) gives

$$\lim_{k\to 0}\frac{I_0'(ka)}{I_0'(kb)} = \frac{a}{b} \tag{2.31}$$

and thus

$$I_s = -I\frac{a^2}{b^2} \tag{2.32}$$

in complete agreement with the result obtained by Turner and Bowley (see Eq. 25 of reference [9]).

2.3 Sine-phi surface current distribution on an infinite cylinder

It is a well known fact that a perfectly homogeneous transverse magnetic field can be generated inside a cylindrical volume using an infinitely long surface current of the form $F_z \propto \sin(\varphi)$ flowing on the cylinder surface in the longitudinal (or z) direction (see [4], [6] or [1]). This sine-phi distribution forms the conceptual basis for transverse B_1 field generation in many NMR and MRI applications. Our interest is in determining the corresponding shielding current distribution $f_z(\varphi, z)$ that eliminates the magnetic field for $\rho > b$. The geometry of this problem is summarized in Fig. 2.3.

To begin, consider the infinitely long current distribution

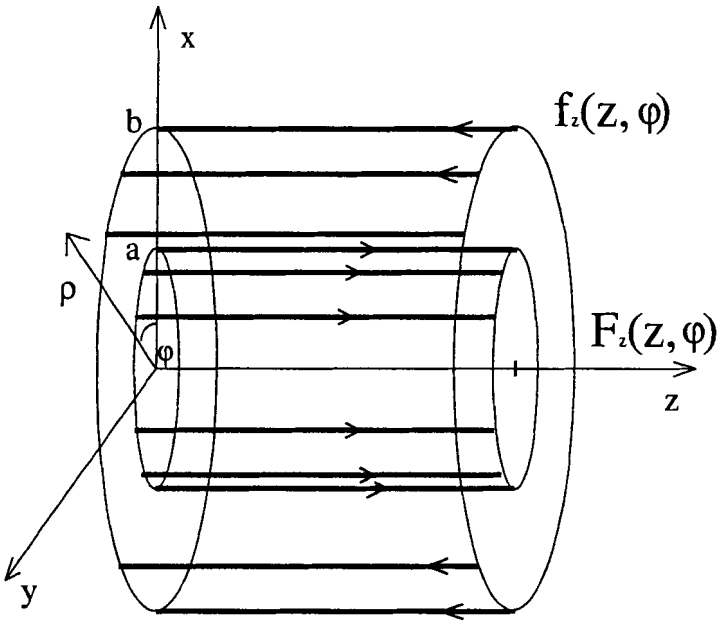

Figure 2.3: Sine-phi current distribution $F_z(\varphi, z)$ on a cylinder of radius a, and the corresponding shielding current distribution $f_z(\varphi, z)$ on a cylinder of radius b.

$$F_z(z, \varphi) = I \sin(\varphi) \tag{2.33}$$

$$F_\varphi(z, \varphi) = 0 \tag{2.34}$$

restricted to the cylinder with $\rho = a$. The Fourier transform of this current sheet is:

$$F_z^m(k) = -im\pi I \delta(k) \delta_{m,\pm 1} \, . \tag{2.35}$$

Making use of Eq. 2.22, the Fourier transformed shielding current distribution

$$f_z^m(k) = -im\pi I \frac{a^2}{b^2} \frac{I'_m(ka)}{I'_m(kb)} \delta(k) \delta_{m,\pm 1} \tag{2.36}$$

is obtained. The inverse transform of Eq. 2.36 gives the shielding current distribution:

$$f_z(\varphi,z) = i\pi I\frac{a^2}{2\pi b^2}\left[-\exp(-i\varphi)\frac{I'_{-1}(ka)}{I_{-1}(kb)} + \exp(i\varphi)\frac{I'_1(ka)}{I'_1(kb)}\right]\Bigg|_{k=0} \tag{2.37}$$

from which

$$f_z(\varphi,z) = -I\sin(\varphi)\frac{a^2}{b^2}\frac{I'_1(ka)}{I'_1(kb)}\Bigg|_{k=0} \tag{2.38}$$

and finally

$$f_z(\varphi,z) = -I\sin(\varphi)\frac{a^2}{b^2}\,. \tag{2.39}$$

Comparing this result for the shielding current distribution $f_z(\varphi,z)$ with the original sine-phi current distribution $F_z(z,\varphi)$ (Eq. 2.33) it is evident that they have the same angular dependence, but flow in opposite directions. The magnitude of the central field scales as $1-a^2/b^2$.

2.4 Analytic approach for shielding two infinitely long wires

Consider the case of two infinitely long wires I^α and I^β carrying the same current I but flowing in opposite directions parallel to the z-axis of a cylindrical coordinate system. Let's arrange them so that the wires are at the positions $\rho = a$ and $\varphi_1 = 0$ and $\varphi_2 = \pi$ as shown in Fig. 2.4. In effect these wires form a rectangular current loop for which the return paths have been moved to $z \to \pm\infty$.

Clearly the total z-component of the current

$$I_z = I_z^\alpha - I_z^\beta \tag{2.40}$$

flowing on the surface of the cylinder at $\rho = a$ is zero. The individual currents $I_z^{\alpha(\beta)}$ can be associated with current densities $J^{\alpha(\beta)}$ such that

$$I_z^{\alpha(\beta)} = \int_0^{2\pi}\int_0^{\infty} J^{\alpha(\beta)}\rho d\rho d\varphi = \int_0^{2\pi}\int_0^{\infty}\frac{I^{\alpha(\beta)}}{a}\delta(\varphi_{\alpha,\beta})\delta(\rho-a)\rho d\rho d\varphi\,. \tag{2.41}$$

In the context of Turner and Bowley's analysis we infer:

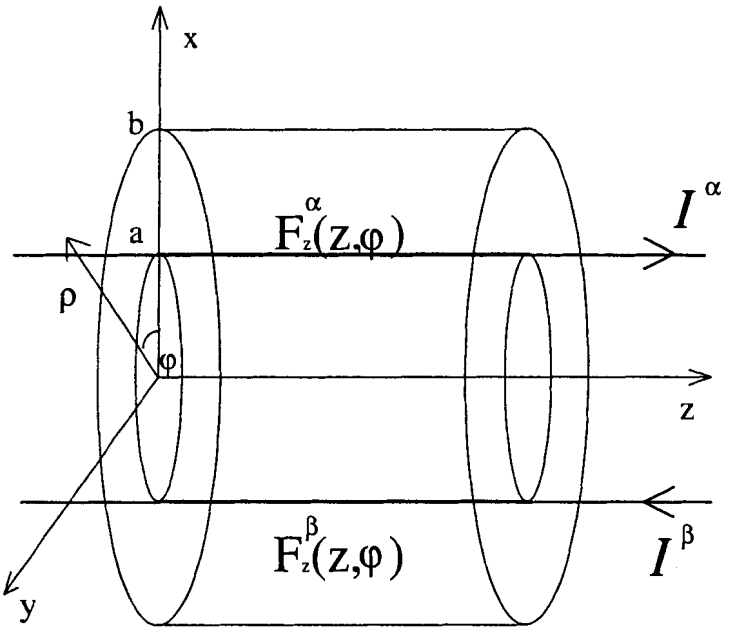

Figure 2.4: An infinitely long system of two current-carrying wires parallel to but offset from the axis of a cylindrical coordinate system.

$$I_z^{\alpha} = \int_0^{2\pi} d\varphi \int_0^{\infty} \delta(\varphi)\delta(\rho - a)\frac{I}{a}\rho d\rho = \int_0^{2\pi} F_z^{\alpha}(\varphi) a d\varphi \tag{2.42}$$

and

$$I_z^{\beta} = \int_0^{2\pi} d\varphi \int_0^{\infty} \delta(\varphi + \pi)\delta(\rho - a)\frac{I}{a}\rho d\rho = \int_0^{2\pi} F_z^{\beta}(\varphi) a d\varphi \tag{2.43}$$

and thus

$$F_z(\varphi) = F_z^{\alpha}(\varphi) + F_z^{\beta}(\varphi) = \frac{I}{a}[\delta(\varphi) - \delta(\varphi + \pi)] \,. \tag{2.44}$$

The φ-component of $F(\varphi)$ is

$$F_\varphi(\varphi) = 0 \,. \tag{2.45}$$

Fourier transformation of F_z^α gives us:

$$F_z^{\alpha,m}(k) = \frac{1}{2\pi}\int_{-\pi}^{\pi} \exp(-im\varphi)\delta(\varphi)d\varphi \int_{-\infty}^{\infty} \exp(-ikz)\frac{I}{a}dz = \frac{I}{2\pi a}\delta(k) \,. \tag{2.46}$$

Substitution of Eq. 2.46 into Eq. 2.22 yields

$$f_z^{\alpha,m}(k) = -I\frac{a}{2\pi b^2}\frac{I'_m(ka)}{I'_m(kb)}\delta(k) \,. \tag{2.47}$$

Finally, inverse Fourier transformation of Eq 2.47 gives a z-directed "shielding" current density at $\rho = b$

$$f_z^\alpha(\varphi) = -\sum_{-\infty}^{\infty} \exp(im\varphi)\int_{-\infty}^{\infty} dk \exp(ikz)\delta(k)\frac{I_z a}{2\pi b^2}\frac{I'_m(ka)}{I'_m(kb)} \,. \tag{2.48}$$

Performing this integral, one finds

$$f_z^\alpha(\varphi) = -\frac{I_z a}{2\pi b^2}\sum_{m=-\infty}^{\infty} \exp(im\varphi)\frac{I'_m(ka)}{I'_m(kb)}\bigg|_{k=0} \tag{2.49}$$

and since [23]

$$I'_m(x) = I'_{-m}(x) \tag{2.50}$$

for modified Bessel functions of any integer order m [23], Eq. 2.49 becomes

$$f_z^\alpha(\varphi) = -\frac{I_z a}{2\pi b^2}\left[\frac{I'_0(ka)}{I'_0(kb)} + 2\sum_{m=1}^{\infty} \cos(m\varphi)\frac{I'_m(ka)}{I'_m(kb)}\right]\bigg|_{k=0} \,. \tag{2.51}$$

In order to proceed further we have evaluate Eq. 2.51 in the limit $k \to 0$. As shown in Appendix A

$$\lim_{k\to 0}\frac{I'_0(ka)}{I'_0(kb)} = \frac{a}{b} \tag{2.52}$$

and Appendix B

$$\lim_{k\to 0}\frac{I'_m(ka)}{I'_m(kb)} = \left(\frac{a}{b}\right)^{m-1} . \tag{2.53}$$

Note that the latter equation is valid for any integer $m \neq 0$.

With these results in hand, $f_z^{\alpha}(\varphi)$ can be rewritten. Substitution of Eqs. 2.52 and 2.53 into Eq. 2.51 leads to

$$f_z^{\alpha}(\varphi) = -\frac{I_z}{2\pi b}\left[\frac{a^2}{b^2} + 2\sum_{m=1}^{\infty}\cos(m\varphi)\left(\frac{a}{b}\right)^m\right] . \tag{2.54}$$

A similar procedure to that outlined above yields:

$$f_z^{\beta}(\varphi) = \frac{I_z}{2\pi b}\left[\frac{a^2}{b^2} + 2\sum_{m=1}^{\infty}\cos(m(\varphi+\pi))\left(\frac{a}{b}\right)^m\right] . \tag{2.55}$$

Now, since the total shielding current is

$$f_z(\varphi) = f_z^{\alpha}(\varphi) + f_z^{\beta}(\varphi) \tag{2.56}$$

we have

$$f_z(\varphi) = -\frac{I_z}{2\pi b}\left[\sum_{m=1}^{\infty}\cos(m\varphi)\left(\frac{a}{b}\right)^m - \sum_{m=1}^{\infty}\cos(m(\varphi+\pi))\left(\frac{a}{b}\right)^m\right] . \tag{2.57}$$

Equation 2.57 represents the exact analytical solution for the surface current $f_z(\varphi)$ on the outer cylinder that completely eliminates the magnetic field $\vec{B}$ produced by two line currents flowing in the opposite direction in the region $\rho > b$.

The analysis presented above suggests that the shielding current density $f_z^{\alpha}(\varphi)$ (or $f_z^{\beta}(\varphi)$), associated with the current I^{α} on the wire at position $\rho = a$ and $\varphi = 0$ (or I^{β} on the wire at $\rho = a$ and $\varphi = \pi$), ought to give the appropriate solution for shielding a single current carrying wire. However, we emphasize that this line of reasoning is faulty. To justify this assertion, consider a region where $\rho >> a$ and b. The sum of the magnetic field produced by a current flowing in a wire and its corresponding shielding current should give $\vec{B} \to 0$ for $\rho > b$. This in turn implies through Ampere's circuital law that the current $I_z^{\alpha} = I$ in the wire and the integrated shielding current density $f_z^{\alpha}(\varphi)$ must sum to zero. Clearly this is not the case since

$$I_z^\alpha = I \neq \int_0^{2\pi} f_z^\alpha(\varphi) b d\varphi = \int_0^{2\pi} \frac{I_z}{2\pi b}\left[\frac{a^2}{b^2} + 2\sum_{m=1}^{\infty}\cos(m\varphi)\left(\frac{a}{b}\right)^m\right] b d\varphi = \frac{a^2}{b^2} I \,. \quad (2.58)$$

The question of how to find the shielding current density $f_z^\alpha(\varphi)$ for a single current I_z^α is considered in the next section.

2.5 Analytic approach to shielding a single long straight wire

It is not possible to apply the Turner and Bowley formulas (Eqs. 2.22 and 2.23) to the problem of a single infinitely long straight wire (see Fig. 2.5). The reason for this is subtle, but important to understand.

Implicit in Turner and Bowley's analysis is the requirement that the current satisfy the equation of continuity

$$\nabla \cdot \vec{J} = 0 \quad (2.59)$$

at all points in space. A single straight current-carrying wire necessarily requires a source and a sink of charges, even if they are located far from the region of interest. That is, the current satisfies an expression of the form

$$\nabla \cdot \vec{J} = -\frac{\partial \rho}{\partial t}\left[\delta(z - z_o) - \delta(z + z_o)\right]_{z_0 \to \infty} \quad (2.60)$$

and hence formulas 2.22 and 2.23 are not valid. Nevertheless, elements of Turner and Bowley's analysis can be applied to this problem, as outlined below.

First, it is clear that the general solution for the shielding current density for a single infinitely long wire at $\rho = a$ and $\varphi = 0$ can not be a function of either ρ or z. That is, the general solution $f_z(z, \rho, \varphi)$ can only be a function g of argument φ:

$$f_z(z, \rho, \varphi) = g_z(\varphi) \,. \quad (2.61)$$

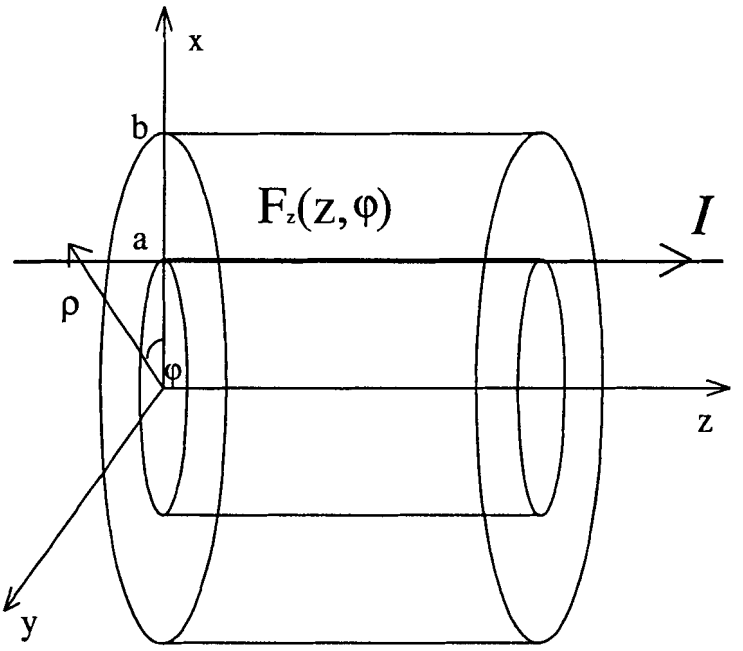

Figure 2.5: An infinitely long current-carrying wire parallel to but offset from the axis of a cylindrical coordinate system.

Second, if one considers the shielding current distribution for two parallel wires (Eq. 2.57, reprinted here)

$$f_z^{(\alpha,\beta)}(\varphi) = -\frac{I_z}{2\pi b}\left[\sum_{m=1}^{\infty}\cos(m\varphi)\left(\frac{a}{b}\right)^m - \sum_{m=1}^{\infty}\cos(m(\varphi+\pi))\left(\frac{a}{b}\right)^m\right] \tag{2.62}$$

it is clear that the angular dependence of the shielding current for a wire at $\rho = a$ and $\varphi = 0$

is completely described by

$$-\frac{I_z}{2\pi b}\sum_{m=1}^{\infty}\cos(m\varphi)\left(\frac{a}{b}\right)^m . \tag{2.63}$$

From this, we infer that

$$g_z(\varphi) = f_z^{\alpha}(\varphi) + const = -\frac{I_z}{2\pi b}\left[\frac{a^2}{b^2} + 2\sum_{m=1}^{\infty}\cos(m\varphi)\left(\frac{a}{b}\right)^m\right] + const . \tag{2.64}$$

Finally, since the total magnetic field produced by the current flowing in the wire and the shielding current flowing on $\rho = b$ must go to zero as $\rho \rightarrow \infty$, the integrated current flowing on $\rho = b$ must be equal to $-I$ (Ampere's circuital law). That is

$$-I \equiv \int_0^{2\pi} g_z(\varphi) b d\varphi = \int_0^{2\pi}\left(-\frac{I_z}{2\pi b}\left[\frac{a^2}{b^2} + 2\sum_{m=1}^{\infty}\cos(m\varphi)\left(\frac{a}{b}\right)^m\right] + const\right) b d\varphi \tag{2.65}$$

from which we infer

$$const = -\frac{I_z}{2\pi b}\left[1 - \frac{a^2}{b^2}\right] \tag{2.66}$$

and finally

$$g_z(\varphi) = -\frac{I_z}{2\pi b}\left[1 + 2\sum_{m=1}^{\infty}\cos(m\varphi)\left(\frac{a}{b}\right)^m\right] . \tag{2.67}$$

In other words, a current density $g_z(\varphi)$ described by Eq. 2.67 will completely eliminate the magnetic field produced by a current I_z flowing in a wire at $\rho = a < b$ and $\varphi = 0$ in the region $\rho > b$.

Chapter 3

Development of a prototype shielded B_1 coil

Cylindrical saddle-shaped coils (see Fig. 3.1) or variations thereof can be used for $\vec{B}_1$ field production in NMR. For these coils, if the length of the coil $l >> 2a$, where a is the radius of the coil, the contribution of the azimuthal current elements to the magnetic field in the central region of interest $(z = l/2)$ is small. It will thus be a good approximation to say that the magnetic field near $z = l/2$ is induced mostly by the current flowing in the axial segments of the coil. This means that as long as the condition $l >> 2a$ is satisfied, the field is reduced to a function of two coordinates (ρ, φ) and Eq. 2.64 (the shielding current distribution $g_z(\varphi)$ for an infinitely long straight wire obtained in the previous chapter) can be employed.

In this chapter numerical calculations are performed for (i) the magnetic fields produced by a long straight wire surrounded by a cylindrical shield, (ii) an array of 10 saddle shaped coils arranged to give a discrete approximation to a sin-phi current distribution, and (iii) a practical implementation of an active shield for the array of saddle-shaped coils. The goal of this exercise is to check for accordance with the analytic expressions derived in Chapter 2. The chapter ends with a description of a prototype coil that was built in order to test its shielding efficacy.

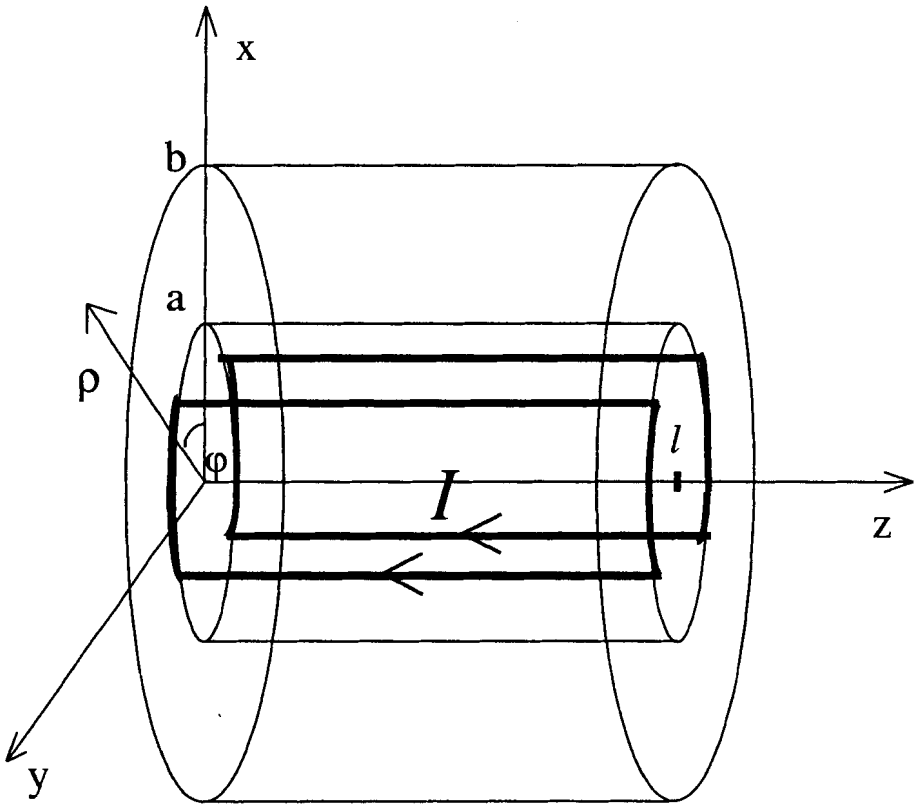

Figure 3.1: The geometry of a cylindrical saddle-shaped coil pair, with length l. The current I produces a transverse magnetic field along the y-direction.

3.1 Numerical calculation of the magnetic field produced by an infinitely-long shielded wire

The geometry of an infinitely long wire surrounded by (but offset from the axis of) a cylindrical conducting shield is relatively simple yet at the same time sufficiently complex to be used as a starting point for performing a numerical check of the accuracy of the derivations presented in Chapter 2. The procedure is straightforward. The appropriate shielding current distribution (Eq. 2.67) is first broken down into filamentary current segments and then, a

vector sum of the magnetic field produced by each of these segments is performed. While this calculation may seem elementary, particularly after the exact analytic result has already been given, in practical terms it was a very important step in building up confidence that our derivations were correct.

For the purpose of numerical calculations, all parameters (i.e. magnetic fields, currents, distances) were written in a non-dimensional form. To illustrate how calculations were set up, let us consider Fig. 3.2. This figure shows the cross section of two concentric cylinders

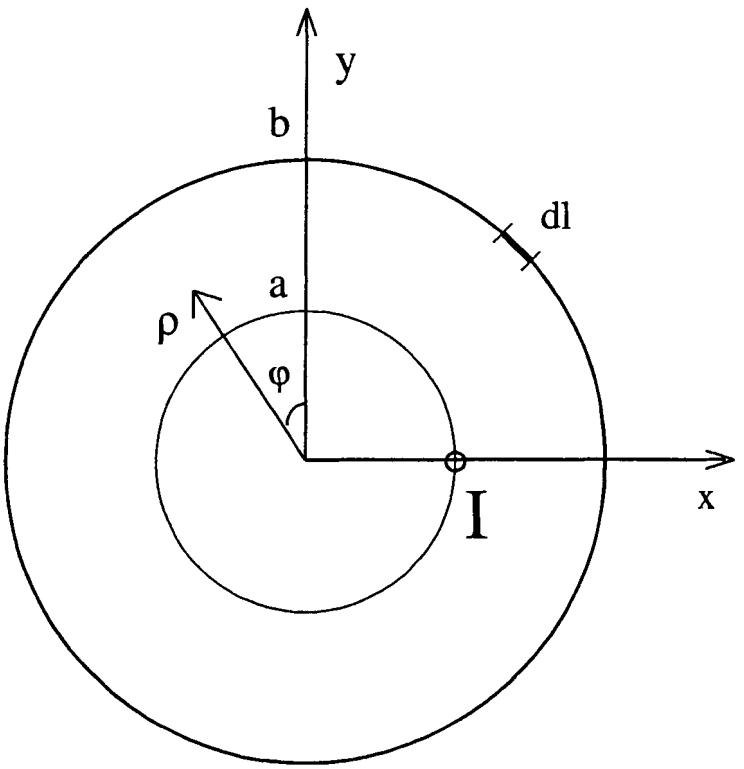

Figure 3.2: The inner current I_{wire} flowing in the z direction is placed at $x_i = a$ and $y_j = 0$ while the shielding current density flowing parallel to the z-axis is spread over the surface of the outer cylinder at $r = b$.

of radii a and b. The current distribution on the inner cylinder consists of an infinitely long straight wire carrying current I_{wire} placed at $x_i = a$ and $y_j = 0$. The shielding current density $I_z(\varphi)$ is distributed over the surface of the outer cylinder at $\rho = b$. Both currents flow parallel to the z-axis which is perpendicular to the page. Knowing the formula for the shielding current density $f_z(\varphi)$ (Eq. 2.67, reproduced here for convenience)

$$f_z(\varphi) = -\frac{I_z}{2\pi b}\left[1+2\sum_{m=1}^{\infty}\cos(m\varphi)\left(\frac{a}{b}\right)^m\right] \tag{3.1}$$

the normalized shielding current $I_i = \frac{I_z(\varphi_i)}{I_{wire}}$ for each arc segment $dl_i = bd\varphi_i$ for the outer cylinder (see Fig. 3.2) can be written:

$$I_i = -\frac{1}{2\pi b}\left[1+2\sum_{m=1}^{\infty}\cos(m\varphi_i)\left(\frac{a}{b}\right)^m\right] dl_i. \tag{3.2}$$

Note here, we assume that each current segment I_i is infinitely long and parallel to the z-axis.

The magnetic fields $\vec{B}_{wire}(x,y)$ produced by I_{wire} and $\vec{B}_i(x,y)$ produced by I_i can be summed to find the total field

$$\vec{B}_{tot}(x,y) = \vec{B}_{wire}(x,y) + \sum_{i=1}^{n}\vec{B}_i(x,y) \tag{3.3}$$

at any point (x,y) using the expression for the magnetic field produced by an infinitely long wire. By increasing the number n of segments dl_i into which the shielding current distribution is split we can increase the accuracy of calculations. Note also that we define the total relative magnetic field at any point to be

$$\frac{\vec{B}_{tot}(x,y)}{\left|\vec{B}_{center}\right|} = \frac{\vec{B}_{wire}(x,y)+\sum_{i=1}^{n}\vec{B}_i(x,y)}{\left|\vec{B}_{center}\right|}. \tag{3.4}$$

The program written to perform these calculations is presented in Appendix C. Figure 3.3 shows the relative value of the shielding current density $f_z(\varphi)$ for the case $a/b = 3/4$. Figure 3.4 shows the corresponding relative magnetic field $|\vec{B}_{tot}|/|\vec{B}_{center}|$ for n=100 shielding current segments. We can clearly see that beyond the outer shielding cylinder, the total magnetic field produced by the current I_{wire} and the shielding currents I_i is $|\vec{B_{tot}}| = 0$ within

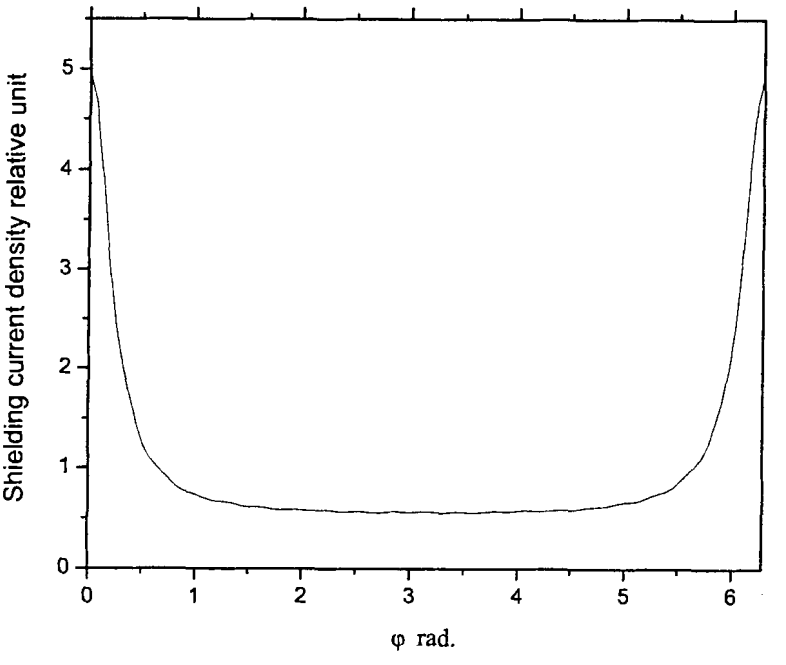

Figure 3.3: Relative value of the shielding current for the case of one wire, with $a/b = 3/4$. Beyond the outer shielding cylinder ($\rho > b$), the magnetic field produced both by current I_{wire} and shielding currents $f(\varphi)$ is $|\vec{B_{tot}}| = 0$.

the accuracy of the numerical calculations. This is in agreement with the analytical result presented in Chapter 2.

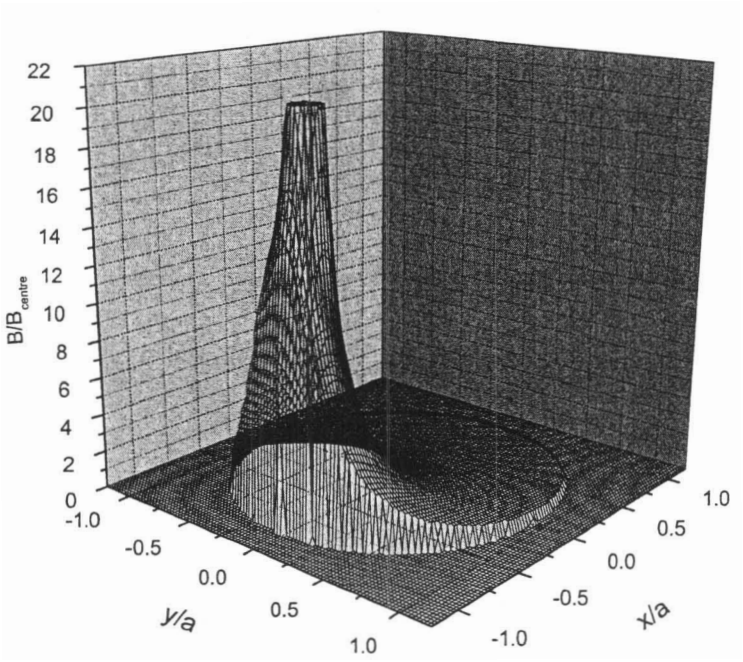

Figure 3.4: Relative value of the magnetic field B/B_{center} for a single shielded wire located such that $a/b = 3/4$ and the number of shielding current segments $n = 100$. Beyond the outer shielding cylinder, the magnetic field produced by the currents is $|\vec{B}_{tot}| = 0$.

3.2 Numerical calculation of the magnetic field produced by a discrete (20 wire) approximation to a sine-phi current distribution

There are a number of challenges associated with producing uniform $\vec{B}_1$ fields in MRI systems. Some approaches to the construction of suitable coils were briefly mentioned in Chapter 1. Previous authors have emphasized that the construction of a coil having a nonuniform sheet current would be very difficult to achieve. In practice, one chooses to approximate a surface current distribution $F(\varphi)$ using an appropriate distribution of some

number of line currents $I(\varphi_i)$. Two well known examples of this are the "sine-phi" coil and the birdcage coil, both of which approximate the field of a uniformly magnetized cylinder through an arrangement of evenly spaced conducting wires that run along the z-axis of the magnet. The current amplitude required in each wire is determined by its angular position φ_i, and must be set to $I_{wire}\sin(\varphi_i)$: for the sine-phi coil this is achieved by using a separate current source for each value $I_{wire}\sin(\varphi_i)$; for the birdcage coil operating at resonance, its circuit is such that the phase of the current I_{wire} flowing in each rung is proportional to φ_i and as a consequence the correct distribution of current is met at any instant in time.

A third possibility is to have all wires carry the same in-phase current $|I_i| = I_{wire}$ but to vary their angular separation so as to best approximate $I(\varphi)$ as illustrated in Fig. 1.1. If we construct a coil using an even number of wires $2n$, the optimal angular positions φ_i for these wires can be set by requiring:

$$\int_{\varphi_i}^{\varphi_{i+1}} I(\varphi)r(\varphi)d\varphi = \frac{1}{n}\int_0^{\pi} I(\varphi)r(\varphi)d\varphi = \frac{1}{n}I_{tot} \tag{3.5}$$

and

$$\int_0^{\varphi_1} I(\varphi)r(\varphi)d\varphi = \frac{1}{2n}I_{tot} \tag{3.6}$$

where $r(\varphi)$ represents the radius of the surface on which the sine-phi current flows. In practice, one only needs to perform this iterative calculation for the first $n/2$ wires within a single quadrant; all other wire positions are then determined by symmetry requirements, with n wires at $\pm\varphi_i$ and n wires at $\pm(180° - \varphi_i)$. For the case of a cylinder, where $r(\varphi) = r$ and $I(\varphi) \sim \sin(\varphi)$, Eqs. 3.5 and 3.6 simplify to:

$$\varphi_1 = \arccos\left(1 - \frac{1}{n}\right) \tag{3.7}$$

and

$$\varphi_{i+1} = \arccos\left(\cos(\varphi_i) - \frac{2}{n}\right). \tag{3.8}$$

For a cylindrical coil with $2n = 20$ wires, Eqs. 3.7 and 3.8 yield the following angles for the first quadrant:

$$\varphi_i = \{25.84°, 45.57°, 60.00°, 72.54°, 84.26°\}\ . \tag{3.9}$$

Numerical calculations of the magnetic field were performed for the particular arrangements of 20 wires described above, in a manner analogous to that described in the previous subsection. The Fortran program for this calculation is presented in Appendix D. The result of the calculation is summarized in Fig. 3.5, which shows the relative magnetic field $\frac{|\vec{B}_{tot}(x,y)|}{|\vec{B}_{center}|}$ as a function of position. The magnetic field in the central region of the coil (i.e.

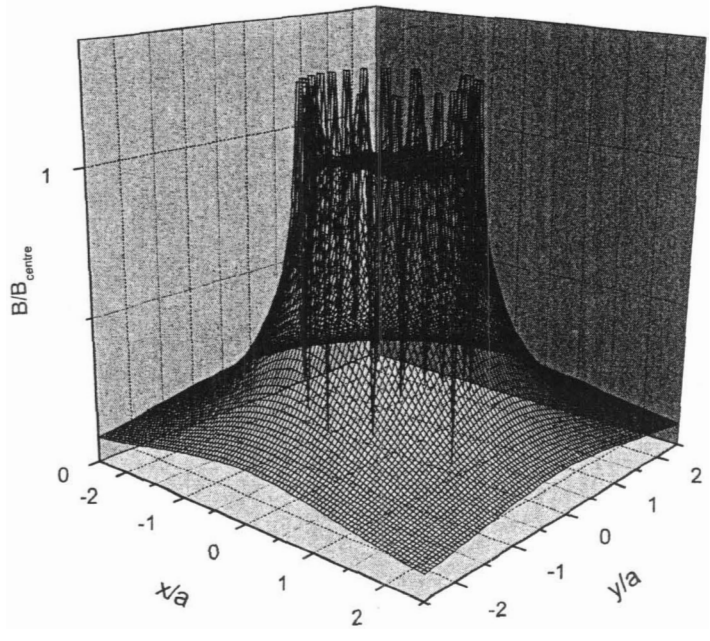

Figure 3.5: Relative value of magnetic field $|\vec{B}/\vec{B}_{center}|$ for a B_1 coil consisting of 20 wires. The field is homogeneous and directed along the x-axis in the central region.

$\rho < a$) is very homogeneous. An active shield for this particular 20-wire coil is described in the following section.

3.3 Geometry for a practical shielded cylindrical B_1 coil

As shown in section 2.5 and illustrated in section 3.1, the magnetic field produced by a current I_{wire} flowing along a wire on the surface of a cylinder at $\rho = a$ can be made identically zero for $\rho > b$ by causing an appropriate current density $f(\varphi)$ to flow on a cylinder at $\rho = b$. Once the positions of 20 wires, each carrying current $|I_i| = I_{wire}$ and placed on the inner cylinder of a B_1 coil have been defined as described in section 3.2, the necessary shielding current density on an outer cylinder $f_{tot}(\varphi)$ is simply

$$f_{tot}(\varphi) = \sum_{i=1}^{20} f_i(\varphi) \tag{3.10}$$

where i identifies a particular wire associated with the B_1 coil, and $f_i(\varphi)$ is the shielding current density on the outer cylinder corresponding to that wire. Using the formula for the shielding current density for an infinitely long current $f_z(\varphi)$ (Eq. 2.67), the total shielding current density $f_{tot}(\varphi)$ can be written

$$f_{tot}(\varphi) = -\sum_{i=1}^{20} \frac{I_i}{2\pi b}\left[1 + 2\sum_{m=1}^{\infty} \cos(m(\varphi+\varphi_i))\left(\frac{a}{b}\right)^m\right] \tag{3.11}$$

where φ_i has the meaning outlined in the previous section (see Eq. 3.9).

A program was written (see Appendix E) to calculate the angular dependence of the continuous shielding current density $f_{tot}(\varphi)$ and the relative magnetic field $\frac{\vec{B}_{tot}(x,y)}{|\vec{B}_{center}|}$ for an array of 20 wires arranged as described in section 3.2. The results of calculations performed by setting $a/b = 4/5$ and restricting m to values $m \leq 100$ are shown in Fig. 3.6 and Fig. 3.7. Comparison of Fig. 3.7 with Fig. 3.5 clearly illustrates the efficiency of the shield.

As was the case in coming up with a discrete approximation to a sine-phi current distribution, we are interested in a discrete approximation to the shielding current distribution $f_{tot}(\varphi)$ shown in Fig. 3.6. Some additional practical constraints that need to be considered are:

1. The wires associated with the B_1 coil and the wires associated with the shield should carry the same in-phase current I_{wire}. This elliminates the need for multiple power supplies and guarantees that inadvertent fluctuations in currents are common to the coil and the shield.

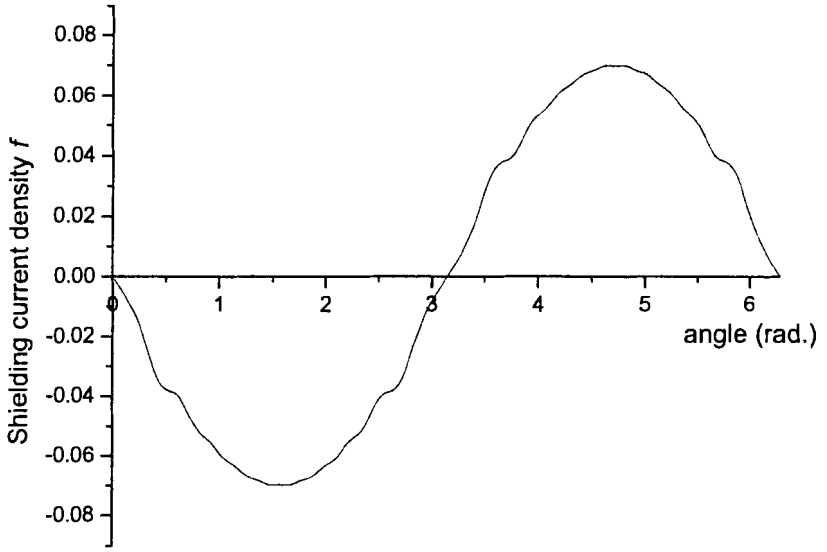

Figure 3.6: Shielding current density $f_{tot}(\varphi)$ (relative units) for a 20-wire B_1 coil, with $a/b = 4/5$.

2. The wires associated with the B_1 coil and those associated with the shield should be as close as possible in order to maximize the volume inside the B_1 coil. Clearly, the field would be zero everywhere if the separation between the coils is reduced to zero, and so some level of compromise is required.

To satisfy these conditions, let us consider the shielding current density $f_z(\varphi,z)$ for a B_1 coil based on a continuous sine-phi current distribution (i.e. Eq. 2.39 reproduced here for convenience):

$$f_z(\varphi,z) = -I\sin(\varphi)\frac{a^2}{b^2}\,. \tag{3.12}$$

For a 20-wire approximation, the current density

$$I = \frac{10I_{wire}}{\pi a} \tag{3.13}$$

and consequently

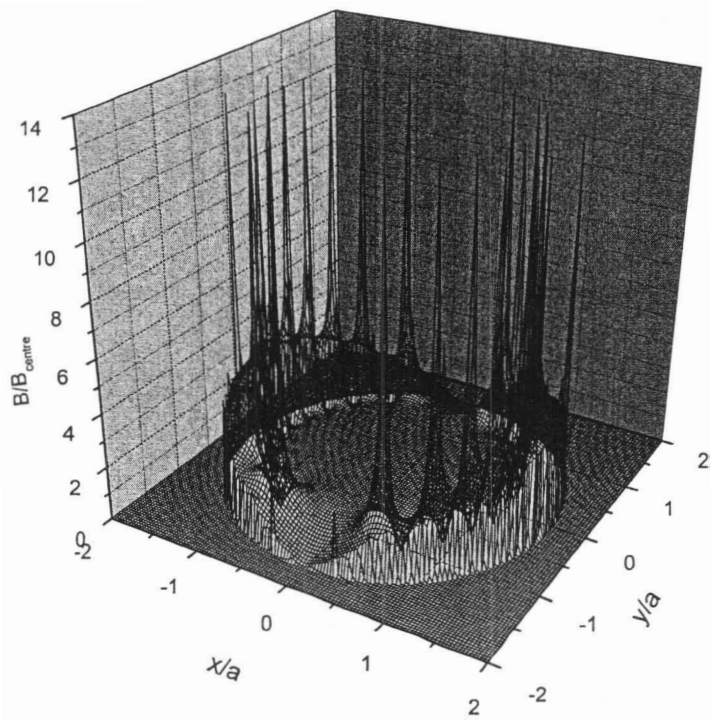

Figure 3.7: Relative magnetic field $\frac{\vec{B}_{tot}(x,y)}{|\vec{B}_{center}|}$ for a shielded 20 wire B_1 coil, for the case of $a/b = 4/5$ and 5000 shield wires.

$$\int_0^{\pi} f_z(\varphi,z) b d\varphi = 10 I_{wire} \frac{a}{b} . \tag{3.14}$$

On the other hand, $f_z(\varphi,z)$ must satisfy

$$\int_0^{\pi} f_z(\varphi,z) b d\varphi = n I_{wire} \tag{3.15}$$

and so n, a, and b must be inter-related such that

$$10 I_{wire} \frac{a}{b} = n I_{wire} \tag{3.16}$$

where n is some integer number ($n < 10$), and a and b are the ρ-coordinates of the inner and outer cylinders. Using Eq. 3.16 and taking into account the conditions outlined above, the

ratio of the radii of the inner ($\rho = a$) and outer ($\rho = b$) cylinders was chosen to be $a/b = 4/5$ for which the total number of shielding wires $m = 2n = 16$.

Once n and a/b are chosen, the final step in defining the geometry of a shield is to calculate the angular positions φ_i^{shield} at which shielding wires should be placed. As was described in section 3.2, we require the shield wires to satisfy

$$\int_{\varphi_i^{shield}}^{\varphi_{i+1}^{shield}} f_{tot}(\varphi) b d\varphi = \frac{1}{2m} I_{tot} \tag{3.17}$$

and

$$\int_0^{\varphi_1} f_{tot}(\varphi) b d\varphi = \frac{1}{2m} I_{tot} \tag{3.18}$$

where $f_{tot}(\varphi)$ is the current distribution plotted in Fig. 3.7. This calculation yields for the first quadrant

$$\varphi_i^{shield} = \{28.0°, 51.0°, 68.01°, 83.0°\} . \tag{3.19}$$

All other wire positions are given by symmetry requirements, with 8 wires at $\pm\varphi_i^{shield}$ and 8 wires at $\pm(180° - \varphi_i^{shield})$.

3.4 Numerical calculation of the magnetic field for a shielded B_1 coil

The previous section outlined the design of a practical shielded cylindrical B_1 coil. A numerical calculation of the field produced by such a coil was performed in a manner analogous to that outlined in sections 3.1 and 3.2. The relevant code is presented in Appendix F. Figure 3.8 shows the relative magnitude of the field $|\vec{B}_{x,y}|/|\vec{B}_{center}|$ produced by this coil. The spikes corresponding to the wire positions have been truncated in order to emphasize that the central field is homogeneous and that the field outside the coil (i.e. $\rho > b$) is sharply attenuated. These results confirm that the geometry described in section 3.3 is suitable for construction of a prototype shielded B_1 coil.

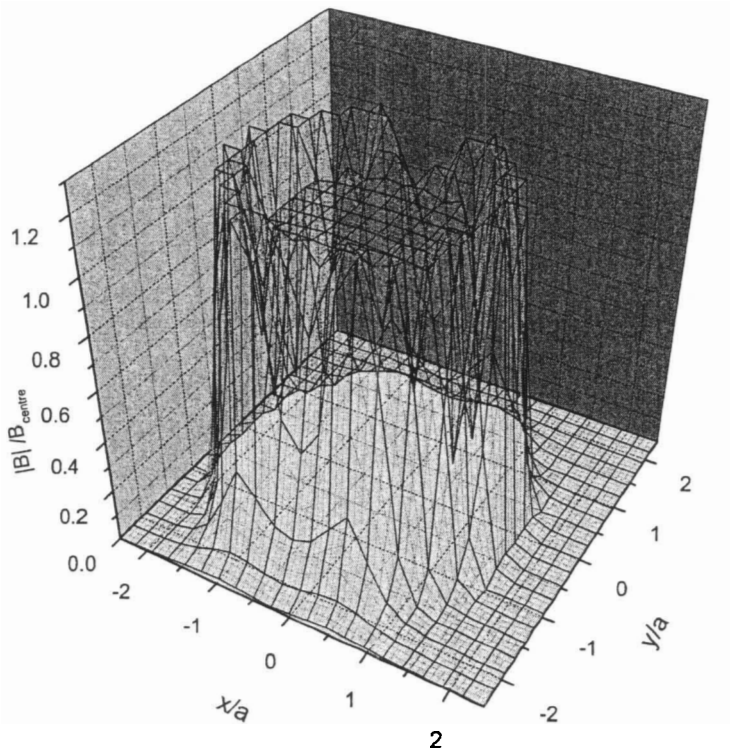

Figure 3.8: Absolute value of magnetic field $|\vec{B}|/|\vec{B_{center}}|$ for a 20-wire B_1 coil shielded by an additional 16 wires.

3.5 Description of a prototype shielded B_1 coil

The shielded B_1 coil described below and shown in Fig. 3.9 was designed to fit inside a solenoidal low-field MRI magnet with an inner diameter ≈ 55 cm. The outer radius of the shielding B_1 coil was thus selected as $b = 27$ cm and in turn $a = (4/5)b = 21.6$ cm. The angular positions of the wires φ_i and φ_i^{shield} are as defined in sections 3.2 and 3.3. The frame of the coil was made from pressed wood in order to be both non-magnetic and non conducting. The length of the coil was set to $l = 1.55$ m, which is longer than the length of the magnet. A single contiguous wire was wound on the frame in order to form the appropriate current paths for the 20-segment inner B_1 coil and the 16-segment outer shield. A break was inserted so that the inner (B_1 coil) and outer shielding coil could be

driven (engaged) independently if desired. Experiments to characterize the magnetic field produced by this prototype shielded B_1 coil are described in the next chapter. Note that the flat surface located both inside and outside of the coil at mid-height corresponds to the plane over which these measurements were performed.

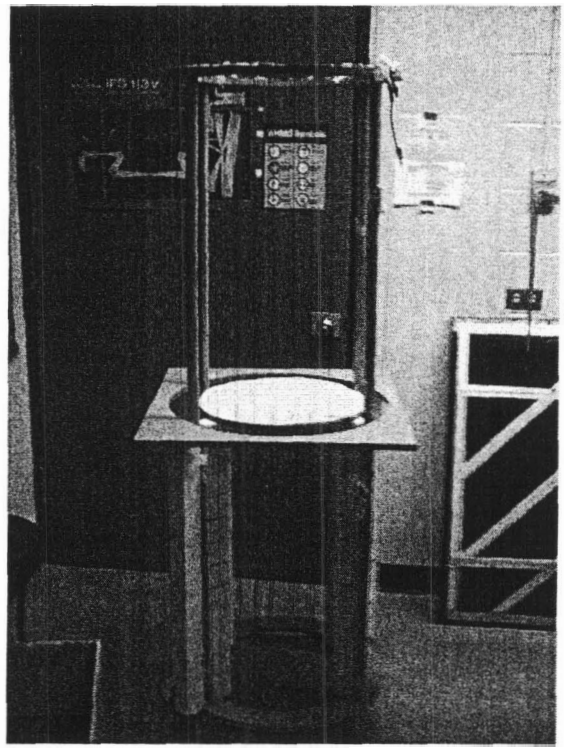

Figure 3.9: The prototype shielded 20 wire $\vec{B}_1$ coil

Chapter 4

Experiments: active shielding

The results presented in Chapter 2 of this thesis were in effect derived from first principles. There is no reason to doubt their validity beyond some inadvertent mathematical error. Given the apparent agreement between these analytic expressions and the numerical computations presented in Chapter 3, it is very unlikely that an error was introduced. Nevertheless, it is only through the construction and characterization of a prototype that a full evaluation of an actively shielded B_1 coil can be performed. In this chapter, the magnetic field produced both inside and outside of the coil described at the end of Chapter 3 is measured and compared with numerical calculations.

First, a technique for measuring an oscillating magnetic field is described, then this technique is applied to the measurement of the field produced by the prototype shielded B_1 coil. Three cases are considered: First, the oscillating magnetic field produced by the prototype shielded B_1 coil is characterized in free space. Next, the influence of conducting objects with the potential to perturb the homogeneity of the field inside the coil is examined. Finally, the prototype is inserted into the bore of a low-field MRI system in order to evaluate the effective inductive decoupling between the B_1 coil and the numerous other coils present in this complex environment that results from the use of the shield.

4.1 Measurement techniques, devices and regimes

As described in Chapter 1, Larmor frequencies $f = \frac{\omega}{2\pi}$ associated with very-low field MRI applications are typically in the range 10 to 300 kHz. The measured inductances of the inner (L_{B_1}) and outer (L_{shield}) windings of the prototype B_1 coil are of order 100 μH. The corresponding reactances $X_L = \omega L$ are of order 100 Ω at $\omega \approx 100$ kHz. The resistance of the coil $R \approx 1.0\ \Omega$. So, we expect that when an oscillating emf

$$\mathcal{E} = \mathcal{E}_0 \cos(\omega t) \tag{4.1}$$

is applied across the coil, a current

$$I_0 = \frac{\mathcal{E}_0}{\sqrt{R^2 + (\omega L)^2}} \tag{4.2}$$

will flow. If $\mathcal{E}_0$ is of order 1 V then we expect $I_0 \gtrsim 10$ mA. This current generates a magnetic field

$$\vec{B}_1 = \vec{B}_1^0 \cos(\omega t) \tag{4.3}$$

inside the coil. For a sine-phi coil with $N = 20$ wires, B_1^0 is approximately twenty times greater than the field produced at distance a from an infinitely long wire. That is,

$$B_1^0 \approx 20 \frac{\mu_0 I_0}{2\pi a} \tag{4.4}$$

which for $a = 0.3$ m and $I_0 = 10$ mA gives $B_1^0 \approx 0.1\ \mu$T.

To detect this field, the emf induced in a coil can be used. The particular coil used here consists of $n = 40$ turns of wire with a radius $r = 10$ mm. The magnetic flux $\Phi(t)$ through the receiver coil due to the $\vec{B}_1$ field is

$$\Phi(t) = \int \vec{B}_1^0 \cos(\omega t) \cdot d\vec{A} = B_1^0 \pi r^2 \cos(\omega t) \tag{4.5}$$

when the coil normal is parallel to the field. This generates an emf

$$\mathcal{E}_{receiver}(t) = -n \frac{d\Phi}{dt} = n B_1^0 \pi r^2 \omega \sin(\omega t) = \mathcal{E}^0_{receiver} \sin(\omega t). \tag{4.6}$$

across the receiver coil. Using the values $B_1^0 = 0.1\ \mu$T and $r = 10$ mm, the emf across the receiver coil should be about 10 mV at 100 kHz. That is an alternating emf $\mathcal{E}_0 = 1$ V applied across the prototype B_1 coil should generate an emf $\mathcal{E}^0_{receiver} \approx 10$ mV across the receiver coil. For the purpose of measuring this emf, a lock in amplifier is convenient and has the advantage that accurate measurements may be made even when the signal of interest is obscured by noise sources that are many thousands of times larger in amplitude [24].

Lock-in amplifiers use a technique known as phase-sensitive detection to measure the amplitude and phase of a component of a signal at a specific reference frequency. Noise signals at frequencies other than the reference frequency are rejected and do not influence the measurement. The particular lock-in amplifier used in these experiments (Stanford Research model SR830) generates an internal reference signal $V_{ref}\sin(\omega_{ref}t + \theta_{ref})$ that can also be used to drive the B_1 coil. Then, the SR830 amplifies the signal of interest (in our case the emf induced in the pickup coil) and multiplies it by the reference signal using two phase sensitive detectors (PSD). The output of a PSD is proportional to the product of two sine waves

$$V_{PSD} \propto V_{sig}V_{ref}\sin(\omega_{ref}t + \theta_{ref})\sin(\omega_{sig}t + \theta_{sig}) \tag{4.7}$$

or

$$V_{PSD} \propto \frac{1}{2}V_{sig}V_{ref}\cos([\omega_{sig} - \omega_{ref}]t + \theta_{sig} - \theta_{ref}) - \cos([\omega_{sig} + \omega_{ref}]t + \theta_{sig} + \theta_{ref})\ . \tag{4.8}$$

In other words, the PSD outputs two AC signals, one at the difference frequency $(\omega_{sig} - \omega_{ref})$ and the other at the sum frequency $(\omega_{sig} + \omega_{ref})$. If the PSD output is fed through a low pass filter, the higher-frequency component of the signal is removed. If ω_{ref} equals ω_{sig}, the difference frequency component will be a DC signal and the filtered PSD output will be

$$V_{PSD} \propto \frac{1}{2}V_{sig}V_{ref}\cos(\theta_{sig} - \theta_{ref})\ . \tag{4.9}$$

If the second PSD multiplies the signal by the reference oscillator signal shifted by 90° (i.e. $V_{ref}(t) \propto V_{ref}\sin(\omega_{ref}t + \theta_{ref} + 90°)$) the DC component of the signal will be

$$V_{PSD2} \propto \frac{1}{2} V_{sig} V_{ref} \sin(\theta_{sig} - \theta_{ref}) \,. \tag{4.10}$$

Once we have these two signals (i.e. $V_{PSD} \propto V_{sig} \cos(\theta_{sig} - \theta_{ref})$ and $V_{PSD2} \propto V_{sig} \sin(\theta_{sig} - \theta_{ref})$ we can calculate V_{sig}:

$$V_{sig} \propto (V_{PSD}^2 + V_{PSD2}^2)^{\frac{1}{2}} \tag{4.11}$$

and the phase difference $\theta = (\theta_{sig} - \theta_{ref})$ between the signal under investigation and the reference signal:

$$\theta = \tan^{-1}\left(\frac{V_{PSD2}}{V_{PSD}}\right) \,. \tag{4.12}$$

Measurements were performed at a frequency of 100 kHz, where the freespace wavelength of electromagnetic radiation is $\lambda = 3$ km. This is long enough that the total length of wire used in fabricating the prototype B_1 coil ($L \approx 60$ m) is only 2% of λ, and thus we expect the current flowing in each rung of the coil to be in phase.

At this point the only remaining question is how to orient the plane of the receiver coil perpendicular to the oscillating magnetic field at every point at which the field is to be measured. In general, one could rotate the receiver coil until maximum in the detected signal is observed, at which point the direction of the normal to the plane of the receiver coil would be parallel to the magnetic field. This procedure is time consuming and requires that many (different) angles be measured accurately.

A simple and less time consuming method for measuring the $\vec{B}_1(x,y)$ field is summarized in Fig. 4.1. It is very easy to orient the receiver coil in the same direction for any (x,y) coordinate in the region of interest and thereby measure the projection of $\vec{B}_1(x,y)$ on this direction. Once projections of $\vec{B}_1(x,y)$ on two axes x' and x'' oriented at an angle of let's say 30° with respect to each other are measured, the original $\vec{B}_1(x,y)$ vector can easily be determined. For example, if the projection of $\vec{B}_1(x,y)$ on the x'-axis is $B_{x'}(x,y)$ and the projection of $\vec{B}_1(x,y)$ on the x''-axis is $B_{x''}(x,y)$ (see Fig 4.1) then

$$B_{x'}(x,y) = \left|\vec{B}_1(x,y)\right| \cos(\alpha)$$
$$B_{x''}(x,y) = \left|\vec{B}_1(x,y)\right| \cos(\beta)$$

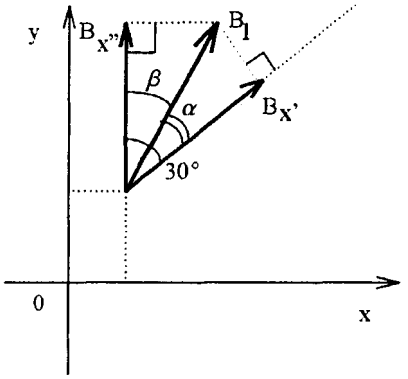

Figure 4.1: The calculation of $\vec{B}_1(x,y)$ using projections of the field onto two axes x' and x'' oriented at an angle of 30° with respect to each other.

where α and β are the angles between $\vec{B}_1(x,y)$ and the two coordinate systems and $\alpha+\beta = 30°$ by construction. From this

$$\beta = \tan^{-1}\left(\frac{\frac{B_{x'}(x,y)}{B_{x''}(x,y)} - \cos(30°)}{\sin(30°)}\right) \tag{4.13}$$

and

$$\left|\vec{B}_1(x,y)\right| = \frac{B_{x''}(x,y)}{\cos(\beta)} . \tag{4.14}$$

In practice this procedure gives very small ($< 0.5\%$) random errors in the determination of $\left|\vec{B}_1(x,y)\right|$ and gives $\vec{B}_1(x,y)$ independent of an absolute determination of the angle between the normal to the plane of the receiver coil and the true direction of the oscillating magnetic field. It has been used for all of the experiments described in the following sections.

4.2 Characterization of the magnetic field produced by the prototype shielded B_1 coil

Measurements of the magnetic field produced both inside and outside of the prototype coil were first performed in free space (i.e. far from perturbing objects) in the plane $z = l/2$ where l is the length of the coil (see Fig. 3.9). The B_1 coil was driven with 5 V, 100 kHz signal and the emf induced in the receiver coil was measured in two orientations 30° apart as described in section 4.1.

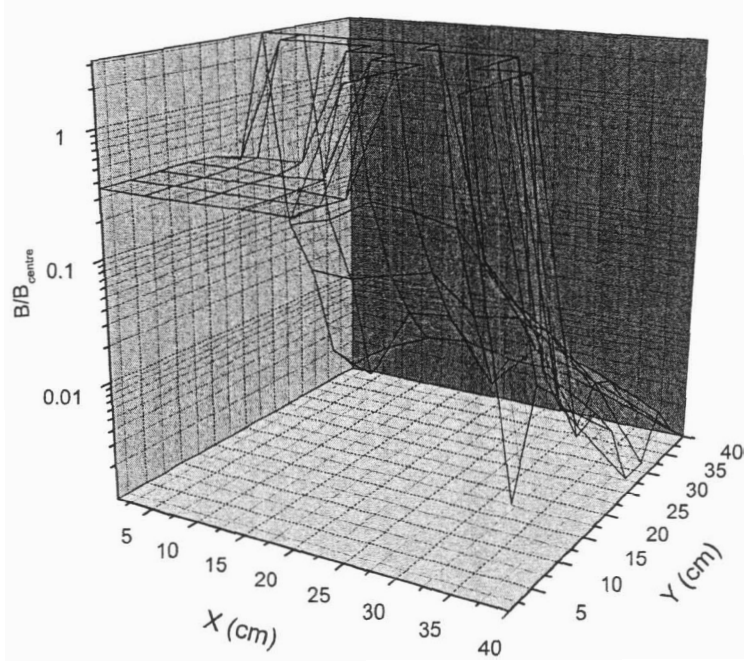

Figure 4.2: Relative magnitude of the field produced by the prototype B_1 coil in free space when the shield is engaged (ON). Results are shown for the first quadrant only for the sake of clarity. Note the logarithmic scale. The value of B_{centre} used here is taken from measurements performed with the shield OFF (see Fig. 4.3) to properly show the influence of the shield.

The measured relative magnitude of the magnetic field $\vec{B}_1(x,y)$ is plotted in Figs 4.2 and 4.3 for the cases when shield is "ON" and "OFF". Several features of these plots are worth

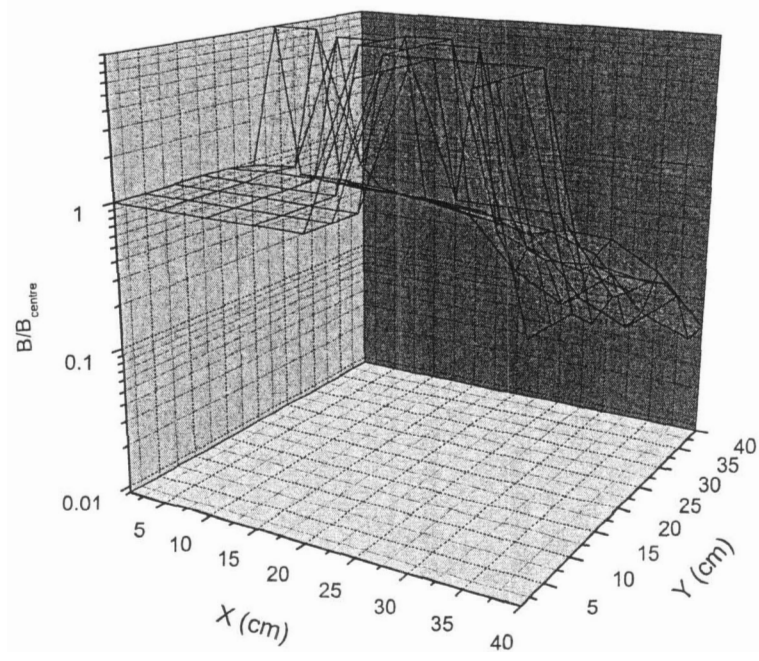

Figure 4.3: Relative magnitude of the field produced by the prototype B_1 coil in free space when the shield is disengaged (OFF). Results are shown for the first quadrant only for the sake of clarity. Note the logarithmic scale.

noting. First, the central field is clearly very homogeneous. The maximum deviation of the field from a constant value is 1.5 % and 1.3 % within a distance $a/2$ of the origin when the shield is ON and OFF, respectively. This compares to a maximum deviation of 1.3 % and 1.1 % for the same two cases predicted by the numerical calculations presented in Chapter 3. Second, the attenuation of the field outside of the coil is much more rapid when the shield is engaged, as expected. The level of attenuation is in agreement with the numerical calculation presented in Chapter 3. And finally third, the magnitude of the central field is

attenuated by a factor 0.646 when the shield is engaged. This compares favorably with the value $a^2/b^2 = 0.64$ expected from theory for an infinitely long coil.

Although only results from the magnitude of $\vec{B}_1(x,y)$ are plotted, the uniformity of the measured field direction is equally impressive. The maximum deviation of the direction of the field from a constant value over the same region is 0.5 ± 0.1 degrees and 0.8 ± 0.1 degrees for the shielded and unshielded cases, respectively.

4.3 Influence of external objects on the internal magnetic field homogeneity

To illustrate the effectiveness of the active shield, the following experiment was performed. A large copper plate measuring 1.5 m $\times$ 1 m was placed near the B_1 coil (see Fig. 4.4). The distance between the coil and the copper plate was set to $a = 5$ cm. The time-varying currents flowing in the rungs of the B_1 coil generate image currents in the copper plate; these image currents in turn influence the magnetic field produced inside the B_1 coil. The emf induced across the receiver coil was measured as a function of position as described previously, both with the shield engaged (ON) and disengaged (OFF). Table 4.3 gives the measured relative deviation of the field

$$\Delta(x) = \left| \frac{B_1(x) - B_1(0)}{B_1(0)} \right| . \tag{4.15}$$

from the central value $B_1(0)$ along the x-axis of Fig. 4.4. The same data are plotted in Fig. 4.5. Also shown in this figure are values of $\Delta(x)$ measured in the absence of the copper plate.

From these data we conclude that the currents induced in the copper plate by the B_1 field disturb the field inside the unshielded coil by a significant amount ($\Delta_{max}^{unshielded} - \Delta_{max}^{infreespace} \approx 14\%$). On the contrary, the B_1 field generated by the shielded coil is almost the same whether or not the copper plate is present ($\Delta_{max}^{shielded} - \Delta_{max}^{infreespace} \approx 0.3\%$), which is in good agreement with our expectations.

X coord. (cm)	$\Delta(x)$ in (%) shielding OFF	$\Delta(x)$ in (%) shielding ON
16	-13.49	-0.129
14	-10.08	1.679
12	-7.977	1.938
10	-6.414	1.421
8	-4.987	0.904
6	-3.668	0.516
4	-2.445	0.129
2	-1.274	0.129
0	0	0
-2	0.866	0.129
-4	1.884	0.387
-6	3.056	0.646
-8	4.024	1.033
-10	5.043	1.679
-12	6.215	2.325
-14	6.979	2.196
-16	6.979	0.129

Table 4.1: Relative deviation $\Delta(x)$ (in %) of the magnetic field along the x-axis of Fig. 4.4 when the copper plate is in position. Data are shown for the cases where the shielding is disengaged (left) and engaged (right).

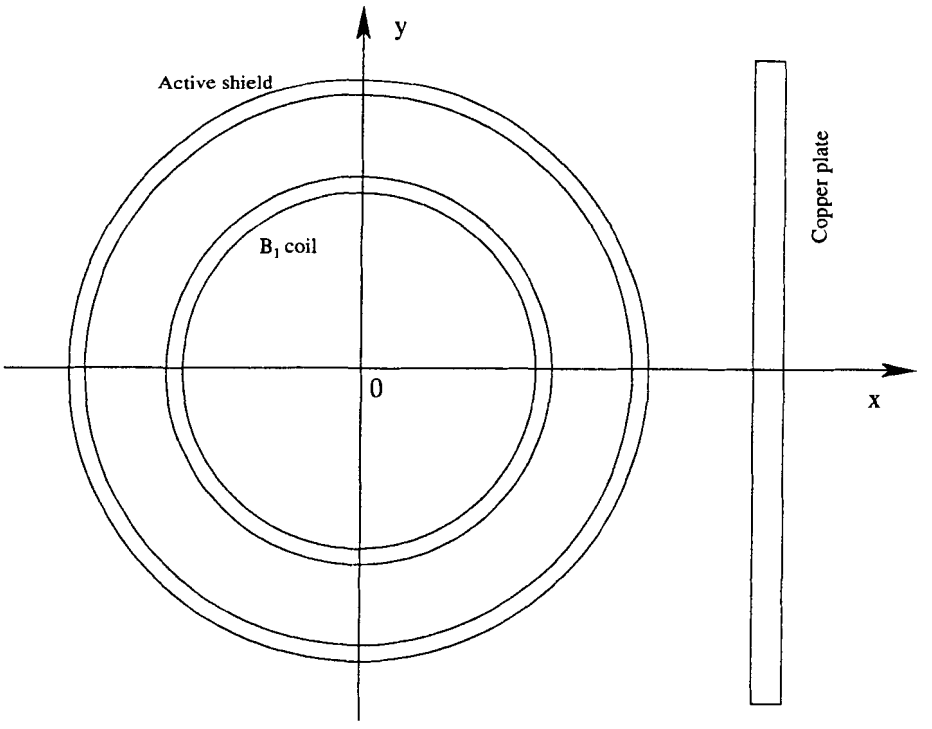

Figure 4.4: The geometry of the experiment used to the test the influence of a perturbing conducting body (a copper plate) on the homogeneity of the internal magnetic field.

4.4 Characterization of the prototype $\vec{B}_1$ coil in a low field MRI magnet

The experiment described in section 4.3 demonstrates the immunity of the shielded B_1 coil to the perturbing influence of external conducting bodies. However, the true test of shielding effectiveness is to place the coil inside a low-field MRI magnet, comprising several dozen coils for producing magnetic fields and fields gradients as well as significant lengths of copper tubing for water cooling of the magnet. The design of the particular magnet used for this test is such that all of these coils are confined to an 8 cm thick shell with an inner diameter of 55 cm; in other words, the MRI magnet presents a complex environment consisting of numerous conducting bodies, all of which are in close proximity to the B_1 coil (see Fig. 4.6).

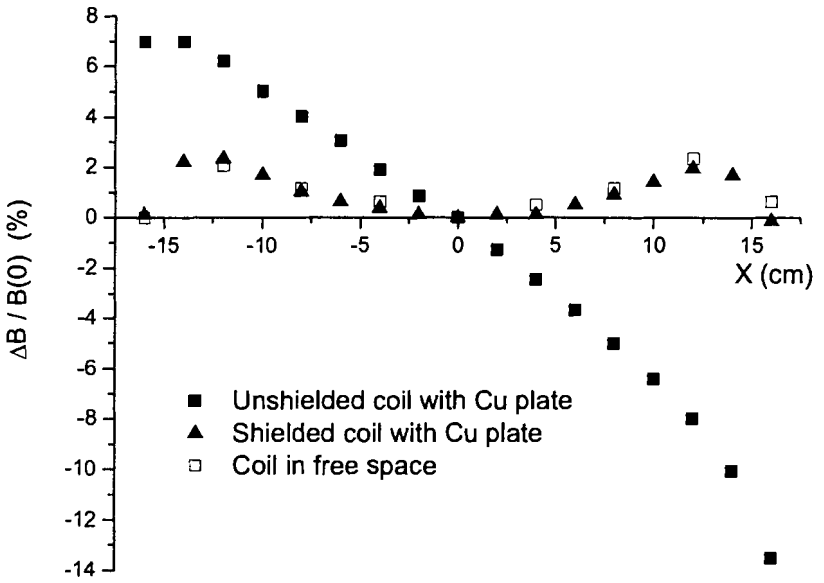

Figure 4.5: Relative deviations $\Delta(x)$ (in %) of the magnetic field along the x-axis of Fig. 4.4 when the copper plate is in position. Data are also shown for the case when the copper plate is removed (shielded coil in free space).

Measurements were performed in a manner analogous to the method described previously. Data for the relative deviation $\Delta(x,y)$ of the field from the central value are reported in tables 4.2 (unshielded) and 4.3 (shielded) and are plotted in Figs. 4.7 (unshielded) and 4.8 (shielded) for a drive frequency of 100 kHz. The difference between these two data sets is clear. The spread in measured values of $\Delta(x,y)$ is significantly larger when the active shielding is disengaged. This is a direct reflection of the complex inductive coupling between the B_1 coil and the MRI magnet.

Engaging the active shield reduces this coupling by attenuating the oscillating magnetic fields produced outside of the central region. There is still a finite spread in measured values of $\Delta(x,y)$ evident in Fig. 4.8, however this can be attributed to the intrinsic homogeneity of

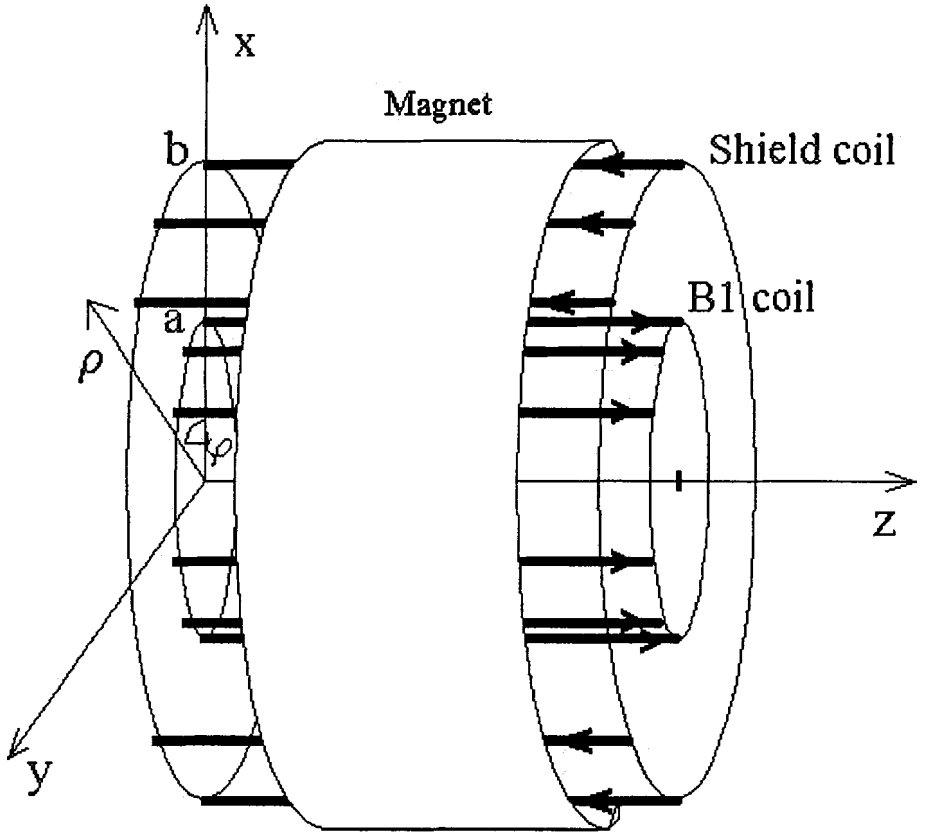

Figure 4.6: Geometry of the experiment to characterize the homogeneity of B_1 fields inside a low-field MRI magnet. The B_1 field is directed along the y-axis.

OFF	x=-8cm	x=-4 cm	0	x=0cm	x=8cm
y=-16	-5.34	-5.09	-5.68	-6.11	-7.40
y=-12	-3.12	-4.35	-3.21	-6.41	-11.10
y=-8	-1.65	0.93	-2.21	-0.83	-0.79
y=0	-1.67	-0.82	0	-0.43	-1.46
y=8	0.41	2.17	4.19	-0.82	-2.61
y=12	10.77	2.16	9.50	-0.74	-10.79
y=16	7.48	4.19	-1.67	-1.19	-5.98

Table 4.2: Relative deviation $\Delta(x)$ (in %) of B_1 from the central value measured in the plane $z = l/2$ when the prototype coil is placed inside the MRI magnet. These data correspond to the case where the active shield is disengaged (OFF).

ON	x=-8cm	x=-4 cm	0	x=0cm	x=8cm
y=-16	3.46	1.96	1.65	2.78	2.83
y=-12	1.36	0.57	0.98	1.36	2.44
y=-8	1.65	0.44	0.13	1.493	1.36
y=0	0.83	0.29	0	0.15	0.49
y=8	1.68	0.47	0.29	0.24	0.47
y=12	2.38	0.97	1.10	0.37	1.96
y=16	3.12	2.62	2.31	0.39	0.97

Table 4.3: Relative deviation $\Delta(x)$ (in %) of B_1 from the central value measured in the plane $z = l/2$ when the prototype coil is placed inside the MRI magnet. These data correspond to the case where the active shield is engaged (ON).

the fields produced by the B_1 coil as calculated in Chapter 3. Further evidence of shielding effectiveness is seen in the symmetry of the measured fields. The data for B_1 shown in Fig. 4.8 reflect the symmetry one expects for a finite length cylindrical sine-phi B_1 coil with azimuthal return paths, while the data shown in Fig. 4.7 do not.

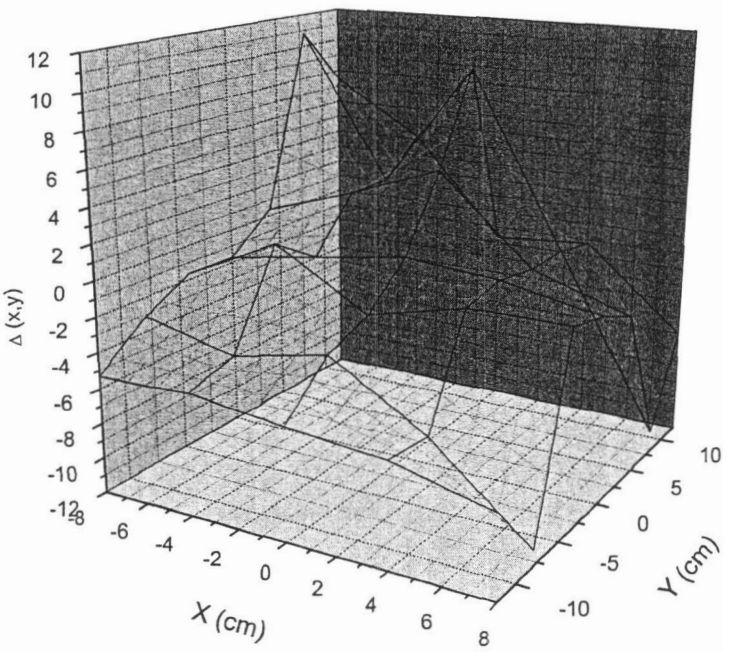

Figure 4.7: Relative deviation $\Delta(x,y)$ of the B_1 field from its central value as measured for the plane $z = l/2$ in Fig. 4.6. These data correspond to the case where the active shield has been disengaged.

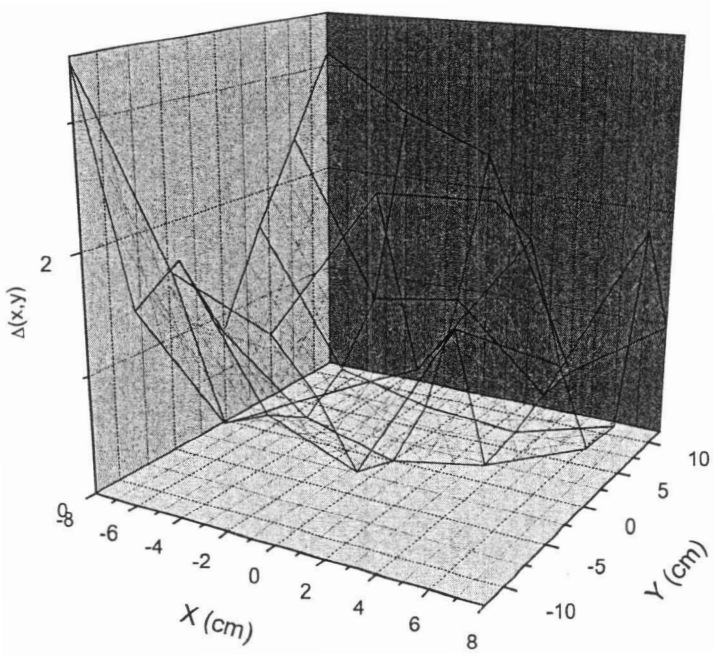

Figure 4.8: Relative deviation $\Delta(x,y)$ of the B_1 field from its central value as measured for the plane $z = l/2$ in Fig. 4.6. These data correspond to the case where the active shield is engaged.

Chapter 5

Discussion

This thesis describes a combined theoretical and experimental study that examines the application of active shielding techniques to the design of transmit (or B_1) coils for low field magnetic resonance imaging. Exact analytic expressions are derived for the current density required to shield the magnetic field produced by a number of elementary coil configurations. Using these analytic results, a prototype shielded B_1 coil based on a sine-phi current distribution was designed and a numerical simulation of the magnetic field it generates was performed. The results of this simulation clearly show that the active shield does indeed sharply attenuate the magnetic field outside of the coil while at the same time retaining the homogeneity of the field produced by the sine-phi B_1 coil. Based on this numerical model, a prototype shielded B_1 coil was constructed and the actual magnetic field it produces was characterized. A key aspect of this experimental work was a series of tests intended to characterize the immunity of the coil to perturbation from external environmental factors such as the presence of conducting bodies.

Ordinarily, passive techniques are used for shielding in NMR and MRI experiments. However, in the low frequency regime these can be awkward to implement. This thesis provides a set of mathematical and conceptual tools for designing actively shielded coils, and demonstrates their utility for low field (low frequency) NMR and MRI as an alternate to passive shielding. The significance of this work is that it demonstrates that actively-shielded B_1 coils do indeed attenuate the influence of external conducting objects (that are necessarily present) on the homogeneity of the magnetic field inside the coil. Actively shielded coils remain useful and straightforward to design as long as one remains in the

quasistatic limit. At higher frequencies phase shifts associated with the finite wavelength of electromagnetic radiation complicate the design process.

A natural extension of the ideas presented in this thesis would be the design of B_1 coils with an elliptical (rather than cylindrical) cross section. This modification would more closely reflect the symmetry of human lungs and might improve the decoupling of the B_1 coil from a B_0 magnet by increasing the distance between the two. While such an extension is technically feasible, the resulting equations are less likely to be as intuitively instructive as those obtained for cylindrical coils.

Apart from low field MRI, another example of a situation where actively-shielded B_1 coils are proving useful is for a new experiment to search for the electric dipole moment of the neutron with unprecidented sensitivity [25]. This experiment, which will involve a complex simultaneous manipulation of neutron and ^{3}He spins, requires that an extremely homogeneous sine-phi coil be operated in a cryogenic environment. The combined requirements of high field homogeneity and low power dissipation (i.e. eddy current heating) make this experiment an ideal candidate for an actively-shielded B_1 coil.

Appendix A

Evaluation of $\frac{I_0'(ka)}{I_0'(kb)}$ as $k \longrightarrow 0$

We wish to evaluate

$$\lim_{k\to 0} \frac{I_0'(ka)}{I_0'(kb)} \,. \tag{A.1}$$

From the recurrence formulas for I_m' (e.g. [23])

$$\left(\frac{1}{z}\frac{d}{dz}\right)^n [z^m I_m(z)] = z^{m-n} I_{m-n}(z) \tag{A.2}$$

we have for $n = 1$ and $m = 0$

$$\left(\frac{1}{z}\frac{d}{dz}\right)^1 [z^0 I_0(z)] = z^{0-1} I_{0-1}(z) \tag{A.3}$$

or

$$\frac{1}{z}\frac{d}{dz}[I_0(z)] = \frac{1}{z} I_{-1}(z) \tag{A.4}$$

so

$$I_0'(z) = I_{-1}(z) \,. \tag{A.5}$$

Thus we are interested in

$$\lim_{k\to 0} \frac{I_0'(ka)}{I_0'(kb)} = \lim_{k\to 0} \frac{I_{-1}(ka)}{I_{-1}(kb)} \,. \tag{A.6}$$

Writing $I_m(z)$ as an infinite series (e.g. [23])

$$I_m(z) = \sum_{l=0}^{\infty} \frac{(z/2)^{m+2l}}{l!\Gamma(m+l+1)} \tag{A.7}$$

leads to

$$I_{-1}(ka) = \sum_{l=0}^{\infty} \frac{(ka/2)^{2l-1}}{l!\Gamma(l)} = \frac{(ka/2)^{-1}}{\Gamma(0)} + \frac{(ka/2)^1}{\Gamma(1)} + \frac{(ka/2)^3}{2\Gamma(2)} \ldots \tag{A.8}$$

for $m = -1$ and $z = ka$. Substitution of Eq. A.8 into Eq. A.6 and keeping in mind that $\frac{1}{\Gamma(0)} \to 0$ gives

$$\lim_{k\to 0} \frac{I_0'(ka)}{I_0'(kb)} = \lim_{k\to 0} \frac{\frac{(ka/2)^1}{\Gamma(1)} + \frac{(ka/2)^3}{2\Gamma(2)} \cdots}{\frac{(kb/2)^1}{\Gamma(1)} + \frac{(kb/2)^3}{2\Gamma(2)} \cdots} \tag{A.9}$$

and thus

$$\lim_{k\to 0} \frac{I_0'(ka)}{I_0'(kb)} = \frac{a}{b} . \tag{A.10}$$

Appendix B

Evaluation of $\frac{I'_m(ka)}{I'_m(kb)}$ as $k \to 0$, for $m \neq 0$

We wish to evaluate

$$\lim_{k\to 0} \frac{I'_m(ka)}{I'_m(kb)} \tag{B.1}$$

for $|m| > 0$. Writing $I_m(x)$ as an infinite series (see for e.g. [23])

$$I_m(x) = \sum_{l=0}^{\infty} \frac{(x/2)^{m+2l}}{l!\Gamma(m+l+1)} \tag{B.2}$$

and differentiating with respect to the argument x yields

$$I'_m(x) = \sum_{l=0}^{\infty} \frac{(m+2l)(x/2)^{m+2l-1}}{l!\Gamma(m+l+1)} . \tag{B.3}$$

Substitution of Eq. B.3 into B.1 gives

$$\lim_{k\to 0} \frac{I'_m(ka)}{I'_m(kb)} = \lim_{k\to 0} \left[\frac{\sum_{l=0}^{\infty} \frac{(m+2l)(ka/2)^{m+2l-1}}{l!\Gamma(m+l+1)}}{\sum_{l=0}^{\infty} \frac{(m+2l)(kb/2)^{m+2l-1}}{l!\Gamma(m+l+1)}} \right] \tag{B.4}$$

and, finally

$$\lim_{k\to 0} \frac{I'_m(ka)}{I'_m(kb)} = \left(\frac{a}{b}\right)^{m-1} . \tag{B.5}$$

Note, that this result is valid only for $m \neq 0$. The corresponding result for $m = 0$ is presented in Appendix A.

Appendix C

Perfectly-shielded wire

Listed below is the Fortran program used to calculate $|\vec{B}/\vec{B}_0|$ for a perfectly-shielded wire. The shielding current distribution is constrained to a cylindrical surface of radius b that is parallel to but offset from the wire by a distance $a < b$. Once the variables a and b are defined, the program calculates the dimensionless ratio $|\vec{B_{tot}}(x,y)|/|\vec{B}_0(x,y)|$ where $B_0(x,y)$ is the magnetic field at point (x,y) due to the wire alone and $\vec{B_{tot}}(x,y)$ is the sum of the field due to the wire and the shield. The results are stored in an array of size dim×dim (in this case 101×101). The central entry in the array (in this case 51,51) is associated with the coordinate $(x = 0, y = 0)$. The program saves the array of $|\vec{B_{tot}}(x,y)|/|\vec{B}_0(x,y)|$ values in the file "fort.1" and the shielding current distribution $f(\varphi_i)$ in the file "fort.2".

```
      real*8 Currnt, Field(1001,1001,2), AbsH(1001,1001)
      real*8 a,b,alfa,c,d,phi,r,cosa,sina,dR,Cur(100)
      integer dim
c     Define parameters
      dim=101
      a=30.
      b=40.
      n=100
      Currnt=0.0
c
      do i=1,1001
       do j=1,1001
        Field(i,j,1)=0.
        Field(i,j,2)=0.
        AbsH(i,j)=0.
c       write(*,*)Field(i,j,1),Field(i,j,1), AbsH(i,j)
        enddo
      enddo
c Calculating the Field from the shielding current Start
      do k=1,n
       phi=k*((2*3.14159265)/n)
       dR=(b*2.*3.14159265)/n
       Currnt=1./(2.*3.14159265*b)
        do l=1,100
```

```
            Currnt=Currnt+(1./(3.14159265))*((a**l)/(b**
     *      (l+l)))*cos(l*phi)
            enddo
            Cur(k)=Currnt
c           write(2,*) Currnt
            do i=1,dim
             do j=1,dim
              d=(((dim-1)/2.)-i)-(b*cos(phi-((2*3.14159265)
     *        /(2*n))))
              c=(((dim-1)/2.)-j)-(b*sin(phi-((2*3.14159265)
     *        /(2*n))))
              r=sqrt((c**2)+(d**2))
              cosa=c/r
              sina=d/r
c             Write(*,*)d,c,' r=',r,' cosa=',cosa,sina
              Field(i,j,1)=Field(i,j,1)+
     *        (((Currnt*dR)/r)*cosa)
              Field(i,j,2)=Field(i,j,2)+
     *        (((Currnt*dR)/r)*sina)
             enddo
            enddo
            write(*,*)  'phi=',phi
c           ' i=',i,' j=',j,
          enddo
c Calculating the Field from the shielding current Finished
c Calculating the Field from the wire on central cylinder
          Current=-1.
            do i=1,dim
              do j=1,dim
                d=(((dim-1)/2.)-i)-a
                c=(((dim-1)/2.)-j)
                r=sqrt((c**2)+(d**2))
                cosa=c/r
                sina=d/r
c               Write(*,*)d,c,' r=',r,' cosa=',cosa,sina
                Field(i,j,1)=Field(i,j,1)+((Current/r)*cosa)
                Field(i,j,2)=Field(i,j,2)+((Current/r)*sina)
c           write(*,*)  'phi=',phi
c           ' i=',i,' j=',j,
              enddo
            enddo
c  Calculating the Field from the wire on central cylinder
c  Finished.

c Calculating Absolute value of the Field. Start
          do i=1,dim
           do j=1,dim
             AbsH(i,j)=sqrt((Field(i,j,1)**2)
     *       +(Field(i,j,2)**2))
             if(AbsH(i,j).gt.0.1) AbsH(i,j)=0.1
c            if(abs(Field(i,j,1)).gt.0.25) Field(i,j,1)=0.25
c            if(abs(Field(i,j,2)).gt.0.25) Field(i,j,2)=0.25
             enddo
          enddo
c Calculating Absolute value of the Field. Finished

c  Printout results for Field. Start
          do i=1,dim
             write(1,555)(AbsH(i,j),j=1,dim)
c            write(3,555)(Field(i,j,2),j=1,dim)
555          FORMAT(10000(1x,F20.15))
          enddo
             write(2,555)(Cur(i),i=1,100)
c   Printout results for Field. Finished
          stop
          end
```

Appendix D

Discrete sine-phi $\vec{B}_1$ coil

Listed below is the Fortran program used to calculate $|\vec{B}/\vec{B}_0|$ for a discrete (20-wire) sine-phi B_1 coil. Once the variable a (the radius of the cylinder on which 20 wires are placed) is defined, the program calculates the dimensionless ratio $|\vec{B_{tot}}(x,y)|/|\vec{B}_0|$ and stores the result in an array of size dim×dim (in this case 101×101). The central entry in the array (in this case 51,51) is associated with the coordinate $(x = 0, y = 0)$. The program saves the array of $|\vec{B_{tot}}(x,y)|/|\vec{B}_0(x,y)|$ values in the file "fort.1".

```
      real*8 Current, Field(1001,1001,2), AbsH(1001,1001)
      real*8 a,b,alfa,c,d,phi,r,cosa,sina,dR,Io
      integer dim

c     Define parameters
      Io=1.
      dim=101
      a=30.
      b=40.
      n=500
      Current=0.0

      do i=1,1001
        do j=1,1001
          Field(i,j,1)=0.
          Field(i,j,2)=0.
          AbsH(i,j)=0.
c         write(*,*)Field(i,j,1),Field(i,j,1), AbsH(i,j)
        enddo
      enddo

        do i=1,dim
         do j=1,dim

c  First quadrant Started
          d=(((dim-1)/2.)-i)-(a*cos(((6.28*25.84)/360.)))
          c=(((dim-1)/2.)-j)-(a*sin(((6.28*25.84)/360.)))
          r=sqrt((c**2)+(d**2))
          cosa=c/r
          sina=d/r
```

```
                Field(i,j,1)=Field(i,j,1)+((Io/r)*cosa)
                Field(i,j,2)=Field(i,j,2)+((Io/r)*sina)
              d=(((dim-1)/2.)-i)-(a*cos(((6.28*45.57)/360.)))
              c=(((dim-1)/2.)-j)-(a*sin(((6.28*45.57)/360.)))
              r=sqrt((c**2)+(d**2))
              cosa=c/r
              sina=d/r
c               Write(*,*)d,c,' r=',r,' cosa=',cosa,sina

                Field(i,j,1)=Field(i,j,1)+((Io/r)*cosa)
                Field(i,j,2)=Field(i,j,2)+((Io/r)*sina)

              d=(((dim-1)/2.)-i)-(a*cos(((6.28*60.)/360.)))
              c=(((dim-1)/2.)-j)-(a*sin(((6.28*60.)/360.)))
                r=sqrt((c**2)+(d**2))
                cosa=c/r
                sina=d/r
c               Write(*,*)d,c,' r=',r,' cosa=',cosa,sina

              Field(i,j,1)=Field(i,j,1)+((Io/r)*cosa)
              Field(i,j,2)=Field(i,j,2)+((Io/r)*sina)
              d=(((dim-1)/2.)-i)-(a*cos(((6.28*72.54)/360.)))
              c=(((dim-1)/2.)-j)-(a*sin(((6.28*72.54)/360.)))
              r=sqrt((c**2)+(d**2))
              cosa=c/r
              sina=d/r
c             Write(*,*)d,c,' r=',r,' cosa=',cosa,sina

              Field(i,j,1)=Field(i,j,1)+((Io/r)*cosa)
              Field(i,j,2)=Field(i,j,2)+((Io/r)*sina)
              d=(((dim-1)/2.)-i)-(a*cos(((6.28*84.26)/360.)))
              c=(((dim-1)/2.)-j)-(a*sin(((6.28*84.26)/360.)))
              r=sqrt((c**2)+(d**2))
              cosa=c/r
              sina=d/r
c             Write(*,*)d,c,' r=',r,' cosa=',cosa,sina

                Field(i,j,1)=Field(i,j,1)+((Io/r)*cosa)
                Field(i,j,2)=Field(i,j,2)+((Io/r)*sina)

c First Quadrant finished

c Second Quadrant Started

          d=(((dim-1)/2.)-i)-(a*cos(((6.28*(180.-25.84))/360.)))
          c=(((dim-1)/2.)-j)-(a*sin(((6.28*(180.-25.84))/360.)))
          r=sqrt((c**2)+(d**2))
          cosa=c/r
          sina=d/r
c         Write(*,*)d,c,' r=',r,' cosa=',cosa,sina

          Field(i,j,1)=Field(i,j,1)+((Io/r)*cosa)
          Field(i,j,2)=Field(i,j,2)+((Io/r)*sina)
          d=(((dim-1)/2.)-i)-(a*cos(((6.28*(180.-45.57))/360.)))
          c=(((dim-1)/2.)-j)-(a*sin(((6.28*(180.-45.57))/360.)))
          r=sqrt((c**2)+(d**2))
          cosa=c/r
          sina=d/r
c         Write(*,*)d,c,' r=',r,' cosa=',cosa,sina

          Field(i,j,1)=Field(i,j,1)+((Io/r)*cosa)
          Field(i,j,2)=Field(i,j,2)+((Io/r)*sina)
          d=(((dim-1)/2.)-i)-(a*cos(((6.28*(180.-60.))/360.)))
          c=(((dim-1)/2.)-j)-(a*sin(((6.28*(180.-60.))/360.)))
          r=sqrt((c**2)+(d**2))
          cosa=c/r
```

```
        sina=d/r
c       Write(*,*)d,c,' r=',r,' cosa=',cosa,sina
        Field(i,j,1)=Field(i,j,1)+((Io/r)*cosa)
        Field(i,j,2)=Field(i,j,2)+((Io/r)*sina)

        d=(((dim-1)/2.)-i)-(a*cos(((6.28*(180.-72.54))/360.)))
        c=(((dim-1)/2.)-j)-(a*sin(((6.28*(180.-72.54))/360.)))
        r=sqrt((c**2)+(d**2))
        cosa=c/r
        sina=d/r
c       Write(*,*)d,c,' r=',r,' cosa=',cosa,sina

        Field(i,j,1)=Field(i,j,1)+((Io/r)*cosa)
        Field(i,j,2)=Field(i,j,2)+((Io/r)*sina)
        d=(((dim-1)/2.)-i)-(a*cos(((6.28*(180.-84.26))/360.)))
        c=(((dim-1)/2.)-j)-(a*sin(((6.28*(180.-84.26))/360.)))
        r=sqrt((c**2)+(d**2))
        cosa=c/r
        sina=d/r
c       Write(*,*)d,c,' r=',r,' cosa=',cosa,sina
        Field(i,j,1)=Field(i,j,1)+((Io/r)*cosa)
        Field(i,j,2)=Field(i,j,2)+((Io/r)*sina)

c Second Quadrant finished

c Third Quadrant Started

        d=(((dim-1)/2.)-i)-(a*cos(((6.28*(180.+25.84))/360.)))
        c=(((dim-1)/2.)-j)-(a*sin(((6.28*(180.+25.84))/360.)))
        r=sqrt((c**2)+(d**2))
        cosa=c/r
        sina=d/r
c       Write(*,*)d,c,' r=',r,' cosa=',cosa,sina
        Field(i,j,1)=Field(i,j,1)+((-Io/r)*cosa)
        Field(i,j,2)=Field(i,j,2)+((-Io/r)*sina)
        d=(((dim-1)/2.)-i)-(a*cos(((6.28*(180.+45.57))/360.)))
        c=(((dim-1)/2.)-j)-(a*sin(((6.28*(180.+45.57))/360.)))
        r=sqrt((c**2)+(d**2))
        cosa=c/r
        sina=d/r
c       Write(*,*)d,c,' r=',r,' cosa=',cosa,sina
        Field(i,j,1)=Field(i,j,1)+((-Io/r)*cosa)
        Field(i,j,2)=Field(i,j,2)+((-Io/r)*sina)
        d=(((dim-1)/2.)-i)-(a*cos(((6.28*(180.+60.))/360.)))
        c=(((dim-1)/2.)-j)-(a*sin(((6.28*(180.+60.))/360.)))
        r=sqrt((c**2)+(d**2))
        cosa=c/r
        sina=d/r
c       Write(*,*)d,c,' r=',r,' cosa=',cosa,sina
        Field(i,j,1)=Field(i,j,1)+((-Io/r)*cosa)
        Field(i,j,2)=Field(i,j,2)+((-Io/r)*sina)
        d=(((dim-1)/2.)-i)-(a*cos(((6.28*(180.+72.54))/360.)))
        c=(((dim-1)/2.)-j)-(a*sin(((6.28*(180.+72.54))/360.)))
        r=sqrt((c**2)+(d**2))
        cosa=c/r
        sina=d/r
c       Write(*,*)d,c,' r=',r,' cosa=',cosa,sina
        Field(i,j,1)=Field(i,j,1)+((-Io/r)*cosa)
        Field(i,j,2)=Field(i,j,2)+((-Io/r)*sina)
        d=(((dim-1)/2.)-i)-(a*cos(((6.28*(180.+84.26))/360.)))
        c=(((dim-1)/2.)-j)-(a*sin(((6.28*(180.+84.26))/360.)))
        r=sqrt((c**2)+(d**2))
        cosa=c/r
        sina=d/r
c       Write(*,*)d,c,' r=',r,' cosa=',cosa,sina
        Field(i,j,1)=Field(i,j,1)+((-Io/r)*cosa)
```

```
        Field(i,j,2)=Field(i,j,2)+((-Io/r)*sina)

c Third Quadrant Finished

c Fourth Quadrant Started
        d=(((dim-1)/2.)-i)-(a*cos(((6.28*(360.-25.84))/360.)))
        c=(((dim-1)/2.)-j)-(a*sin(((6.28*(360.-25.84))/360.)))
        r=sqrt((c**2)+(d**2))
        cosa=c/r
        sina=d/r
c       Write(*,*)d,c,' r=',r,' cosa=',cosa,sina
        Field(i,j,1)=Field(i,j,1)+((-Io/r)*cosa)
        Field(i,j,2)=Field(i,j,2)+((-Io/r)*sina)
        d=(((dim-1)/2.)-i)-(a*cos(((6.28*(360.-45.57))/360.)))
        c=(((dim-1)/2.)-j)-(a*sin(((6.28*(360.-45.57))/360.)))
        r=sqrt((c**2)+(d**2))
        cosa=c/r
        sina=d/r
c       Write(*,*)d,c,' r=',r,' cosa=',cosa,sina
        Field(i,j,1)=Field(i,j,1)+((-Io/r)*cosa)
        Field(i,j,2)=Field(i,j,2)+((-Io/r)*sina)
        d=(((dim-1)/2.)-i)-(a*cos(((6.28*(360.-60.))/360.)))
        c=(((dim-1)/2.)-j)-(a*sin(((6.28*(360.-60.))/360.)))
        r=sqrt((c**2)+(d**2))
        cosa=c/r
        sina=d/r
c       Write(*,*)d,c,' r=',r,' cosa=',cosa,sina
        Field(i,j,1)=Field(i,j,1)+((-Io/r)*cosa)
        Field(i,j,2)=Field(i,j,2)+((-Io/r)*sina)
        d=(((dim-1)/2.)-i)-(a*cos(((6.28*(360.-72.54))/360.)))
        c=(((dim-1)/2.)-j)-(a*sin(((6.28*(360.-72.54))/360.)))
        r=sqrt((c**2)+(d**2))
        cosa=c/r
        sina=d/r
c       Write(*,*)d,c,' r=',r,' cosa=',cosa,sina
        Field(i,j,1)=Field(i,j,1)+((-Io/r)*cosa)
        Field(i,j,2)=Field(i,j,2)+((-Io/r)*sina)
        d=(((dim-1)/2.)-i)-(a*cos(((6.28*(360.-84.26))/360.)))
        c=(((dim-1)/2.)-j)-(a*sin(((6.28*(360.-84.26))/360.)))
        r=sqrt((c**2)+(d**2))
        cosa=c/r
        sina=d/r
c       Write(*,*)d,c,' r=',r,' cosa=',cosa,sina
        Field(i,j,1)=Field(i,j,1)+((-Io/r)*cosa)
        Field(i,j,2)=Field(i,j,2)+((-Io/r)*sina)
c Fourth Quadrant Finished

          enddo
         enddo

c Calculating Absolute Value of the Field
        do i=1,dim
         do j=1,dim
          AbsH(i,j)=sqrt((Field(i,j,1)**2)+(Field(i,j,2)**2))
          if(AbsH(i,j).gt.1.) AbsH(i,j)=1.0
         enddo
        enddo

c  Printout results for Field. Start
        do i=1,dim
           write(1,555)(AbsH(i,j),j=1,dim)
555        FORMAT(10000(1x,F20.15))
        enddo
c   Printout results for Field. Finished
        stop
        end
```

Appendix E

Finely-discretized current distribution

Listed below is the Fortran program used to calculate $|\vec{B}/\vec{B_0}|$ for a discrete (20 wire) sine-phi B_1 coil shielded by a finely-discretized current $f_{tot}(\varphi_i)dl_i$, where $0 \leqslant i \leqslant 5000$ (see Eq. 3.11). Once the variables a and b (the radii of inner and outer cylinders on which the currents flow) are defined, the program calculates the dimensionless ratio $|\vec{B_{tot}}(x,y)|/|\vec{B_0}|$ and stores the results in an array of size dim×dim (in this case 121×121). The central entry in the array (in this case 61,61) is associated with the coordinate $(x = 0, y = 0)$. The program saves the array of $|\vec{B_{tot}}(x,y)|/|\vec{B_0}|$ values in the file "fort.1".

```
      real*8 Current, Field(1001,1001,2), AbsH(1001,1001)
      real*8 a,b,alfa,c,d,phi,r,cosa,sina,dR,Io,Currnt,Cu
      integer dim

c     Define parameters
      Io=1.
      dim=121
      a=40.
c      *sqrt(4./5.)
      b=50.
      n=5000
      Current=0.0
      Currnt=0.0
      Cu=0.0

      do i=1,1001
         do j=1,1001
         Field(i,j,1)=0.
         Field(i,j,2)=0.
         AbsH(i,j)=0.
c         write(*,*)Field(i,j,1),Field(i,j,1), AbsH(i,j)
         enddo
      enddo


c Field for 20 wires. Start
        do i=1,dim
          do j=1,dim
```

```
c  First quadrant Started
         d=(((dim-1)/2.)-i)-(a*cos((((2*3.14159265)
     *  *25.84)/360.)))
         c=(((dim-1)/2.)-j)-(a*sin((((2*3.14159265)
     *  *25.84)/360.)))
         r=sqrt((c**2)+(d**2))
         cosa=c/r
         sina=d/r
         Field(i,j,1)=Field(i,j,1)+((Io/r)*cosa)
         Field(i,j,2)=Field(i,j,2)+((Io/r)*sina)

         d=(((dim-1)/2.)-i)-(a*cos((((2*3.14159265)
     *  *45.57)/360.)))
         c=(((dim-1)/2.)-j)-(a*sin((((2*3.14159265)
     *  *45.57)/360.)))
         r=sqrt((c**2)+(d**2))
         cosa=c/r
         sina=d/r
c        Write(*,*)d,c,' r=',r,' cosa=',cosa,sina

         Field(i,j,1)=Field(i,j,1)+((Io/r)*cosa)
         Field(i,j,2)=Field(i,j,2)+((Io/r)*sina)
         d=(((dim-1)/2.)-i)-(a*cos((((2*3.14159265)
     *  *60.)/360.)))
         c=(((dim-1)/2.)-j)-(a*sin((((2*3.14159265)
     *  *60.)/360.)))
         r=sqrt((c**2)+(d**2))
         cosa=c/r
         sina=d/r
c        Write(*,*)d,c,' r=',r,' cosa=',cosa,sina

         Field(i,j,1)=Field(i,j,1)+((Io/r)*cosa)
         Field(i,j,2)=Field(i,j,2)+((Io/r)*sina)
         d=(((dim-1)/2.)-i)-(a*cos((((2*3.14159265)
     *  *72.54)/360.)))
         c=(((dim-1)/2.)-j)-(a*sin((((2*3.14159265)
     *  *72.54)/360.)))
         r=sqrt((c**2)+(d**2))
         cosa=c/r
         sina=d/r
c        Write(*,*)d,c,' r=',r,' cosa=',cosa,sina

         Field(i,j,1)=Field(i,j,1)+((Io/r)*cosa)
         Field(i,j,2)=Field(i,j,2)+((Io/r)*sina)
         d=(((dim-1)/2.)-i)-(a*cos((((2*3.14159265)
     *  *84.26)/360.)))
         c=(((dim-1)/2.)-j)-(a*sin((((2*3.14159265)
     *  *84.26)/360.)))
         r=sqrt((c**2)+(d**2))
         cosa=c/r
         sina=d/r
c        Write(*,*)d,c,' r=',r,' cosa=',cosa,sina

         Field(i,j,1)=Field(i,j,1)+((Io/r)*cosa)
         Field(i,j,2)=Field(i,j,2)+((Io/r)*sina)

c First Quadrant finished

c Second Quadrant Started

         d=(((dim-1)/2.)-i)-(a*cos((((2*3.14159265)
     *  *(180.-25.84))/360.)))
         c=(((dim-1)/2.)-j)-(a*sin((((2*3.14159265)
     *  *(180.-25.84))/360.)))
         r=sqrt((c**2)+(d**2))
```

```
        cosa=c/r
        sina=d/r
c       Write(*,*)d,c,' r=',r,' cosa=',cosa,sina

        Field(i,j,1)=Field(i,j,1)+((Io/r)*cosa)
        Field(i,j,2)=Field(i,j,2)+((Io/r)*sina)

        d=(((dim-1)/2.)-i)-(a*cos((((2*3.14159265)
     *  *(180.-45.57))/360.)))
        c=(((dim-1)/2.)-j)-(a*sin((((2*3.14159265)
     *  *(180.-45.57))/360.)))
        r=sqrt((c**2)+(d**2))
        cosa=c/r
        sina=d/r
c       Write(*,*)d,c,' r=',r,' cosa=',cosa,sina

        Field(i,j,1)=Field(i,j,1)+((Io/r)*cosa)
        Field(i,j,2)=Field(i,j,2)+((Io/r)*sina)

        d=(((dim-1)/2.)-i)-(a*cos((((2*3.14159265)
     *  *(180.-60.))/360.)))
        c=(((dim-1)/2.)-j)-(a*sin((((2*3.14159265)
     *  *(180.-60.))/360.)))
        r=sqrt((c**2)+(d**2))
        cosa=c/r
        sina=d/r
c       Write(*,*)d,c,' r=',r,' cosa=',cosa,sina

        Field(i,j,1)=Field(i,j,1)+((Io/r)*cosa)
        Field(i,j,2)=Field(i,j,2)+((Io/r)*sina)

        d=(((dim-1)/2.)-i)-(a*cos((((2*3.14159265)
     *  *(180.-72.54))/360.)))
        c=(((dim-1)/2.)-j)-(a*sin((((2*3.14159265)
     *  *(180.-72.54))/360.)))
        r=sqrt((c**2)+(d**2))
        cosa=c/r
        sina=d/r
c       Write(*,*)d,c,' r=',r,' cosa=',cosa,sina

        Field(i,j,1)=Field(i,j,1)+((Io/r)*cosa)
        Field(i,j,2)=Field(i,j,2)+((Io/r)*sina)
        d=(((dim-1)/2.)-i)-(a*cos((((2*3.14159265)
     *  *(180.-84.26))/360.)))
        c=(((dim-1)/2.)-j)-(a*sin((((2*3.14159265)
     *  *(180.-84.26))/360.)))
        r=sqrt((c**2)+(d**2))
        cosa=c/r
        sina=d/r
c       Write(*,*)d,c,' r=',r,' cosa=',cosa,sina

        Field(i,j,1)=Field(i,j,1)+((Io/r)*cosa)
        Field(i,j,2)=Field(i,j,2)+((Io/r)*sina)

c Second Quadrant finished

c Third Quadrant Started

        d=(((dim-1)/2.)-i)-(a*cos((((2*3.14159265)
     *  *(180.+25.84))/360.)))
        c=(((dim-1)/2.)-j)-(a*sin((((2*3.14159265)
     *  *(180.+25.84))/360.)))
        r=sqrt((c**2)+(d**2))
        cosa=c/r
        sina=d/r
c       Write(*,*)d,c,' r=',r,' cosa=',cosa,sina
```

```
        Field(i,j,1)=Field(i,j,1)+(((-1.*Io)/r)*cosa)
        Field(i,j,2)=Field(i,j,2)+(((-1.*Io)/r)*sina)

        d=(((dim-1)/2.)-i)-(a*cos((((2*3.14159265)
     *  *(180.+45.57))/360.)))
        c=(((dim-1)/2.)-j)-(a*sin((((2*3.14159265)
     *  *(180.+45.57))/360.)))
        r=sqrt((c**2)+(d**2))
        cosa=c/r
        sina=d/r
c       Write(*,*)d,c,' r=',r,' cosa=',cosa,sina

        Field(i,j,1)=Field(i,j,1)+(((-1.*Io)/r)*cosa)
        Field(i,j,2)=Field(i,j,2)+(((-1.*Io)/r)*sina)

        d=(((dim-1)/2.)-i)-(a*cos((((2*3.14159265)
     *  *(180.+60.))/360.)))
        c=(((dim-1)/2.)-j)-(a*sin((((2*3.14159265)
     *  *(180.+60.))/360.)))
        r=sqrt((c**2)+(d**2))
        cosa=c/r
        sina=d/r
c       Write(*,*)d,c,' r=',r,' cosa=',cosa,sina

        Field(i,j,1)=Field(i,j,1)+(((-1.*Io)/r)*cosa)
        Field(i,j,2)=Field(i,j,2)+(((-1.*Io)/r)*sina)
        d=(((dim-1)/2.)-i)-(a*cos((((2*3.14159265)
     *  *(180.+72.54))/360.)))
        c=(((dim-1)/2.)-j)-(a*sin((((2*3.14159265)
     *  *(180.+72.54))/360.)))
        r=sqrt((c**2)+(d**2))
        cosa=c/r
        sina=d/r
c       Write(*,*)d,c,' r=',r,' cosa=',cosa,sina

        Field(i,j,1)=Field(i,j,1)+(((-1.*Io)/r)*cosa)
        Field(i,j,2)=Field(i,j,2)+(((-1.*Io)/r)*sina)

        d=(((dim-1)/2.)-i)-(a*cos((((2*3.14159265)
     *  *(180.+84.26))/360.)))
        c=(((dim-1)/2.)-j)-(a*sin((((2*3.14159265)
     *  *(180.+84.26))/360.)))
        r=sqrt((c**2)+(d**2))
        cosa=c/r
        sina=d/r
c       Write(*,*)d,c,' r=',r,' cosa=',cosa,sina

        Field(i,j,1)=Field(i,j,1)+(((-1.*Io)/r)*cosa)
        Field(i,j,2)=Field(i,j,2)+(((-1.*Io)/r)*sina)

c Third Quadrant Finished

c Fourth Quadrant Started

        d=(((dim-1)/2.)-i)-(a*cos((((2*3.14159265)
     *  *(360.-25.84))/360.)))
        c=(((dim-1)/2.)-j)-(a*sin((((2*3.14159265)
     *  *(360.-25.84))/360.)))
        r=sqrt((c**2)+(d**2))
        cosa=c/r
        sina=d/r
c       Write(*,*)d,c,' r=',r,' cosa=',cosa,sina

        Field(i,j,1)=Field(i,j,1)+(((-1.*Io)/r)*cosa)
        Field(i,j,2)=Field(i,j,2)+(((-1.*Io)/r)*sina)
```

```
        d=(((dim-1)/2.)-i)-(a*cos((((2*3.14159265)
     *  *(360.-45.57))/360.)))
        c=(((dim-1)/2.)-j)-(a*sin((((2*3.14159265)
     *  *(360.-45.57))/360.)))
        r=sqrt((c**2)+(d**2))
        cosa=c/r
        sina=d/r
c       Write(*,*)d,c,' r=',r,' cosa=',cosa,sina

        Field(i,j,1)=Field(i,j,1)+(((-1.*Io)/r)*cosa)
        Field(i,j,2)=Field(i,j,2)+(((-1.*Io)/r)*sina)

        d=(((dim-1)/2.)-i)-(a*cos((((2*3.14159265)
     *  *(360.-60.))/360.)))
        c=(((dim-1)/2.)-j)-(a*sin((((2*3.14159265)
     *  *(360.-60.))/360.)))
        r=sqrt((c**2)+(d**2))
        cosa=c/r
        sina=d/r
c       Write(*,*)d,c,' r=',r,' cosa=',cosa,sina

        Field(i,j,1)=Field(i,j,1)+(((-1.*Io)/r)*cosa)
        Field(i,j,2)=Field(i,j,2)+(((-1.*Io)/r)*sina)

        d=(((dim-1)/2.)-i)-(a*cos((((2*3.14159265)
     *  *(360.-72.54))/360.)))
        c=(((dim-1)/2.)-j)-(a*sin((((2*3.14159265)
     *  *(360.-72.54))/360.)))
        r=sqrt((c**2)+(d**2))
        cosa=c/r
        sina=d/r
c       Write(*,*)d,c,' r=',r,' cosa=',cosa,sina

        Field(i,j,1)=Field(i,j,1)+(((-1.*Io)/r)*cosa)
        Field(i,j,2)=Field(i,j,2)+(((-1.*Io)/r)*sina)

        d=(((dim-1)/2.)-i)-(a*cos((((2*3.14159265)
     *  *(360.-84.26))/360.)))
        c=(((dim-1)/2.)-j)-(a*sin((((2*3.14159265)
     *  *(360.-84.26))/360.)))
        r=sqrt((c**2)+(d**2))
        cosa=c/r
        sina=d/r
c       Write(*,*)d,c,' r=',r,' cosa=',cosa,sina

        Field(i,j,1)=Field(i,j,1)+(((-1.*Io)/r)*cosa)
        Field(i,j,2)=Field(i,j,2)+(((-1.*Io)/r)*sina)

c Fourth Quadrant Finished
          enddo
         enddo
c Calculate Field from shield ---

        do k=1,n

         phi=k*((2*3.14159265)/n)
         dR=(b*2.*3.14159265)/n

c 20 Chris's currents
c        Currnt=20.*(1./(2.*3.14159265*b))
         Currnt=0.0

        do l=1,100
        Currnt=Currnt+(1./(3.14159265))*((a**l)/(b**(l+1)))*(
     *  (-1.)*cos(l*(phi-(((2*3.14159265)*25.84)/360.))) -
```

```
     *  cos(l*(phi-(((2*3.14159265)*45.57)/360.))) -
     *  cos(l*(phi-(((2*3.14159265)*60.)/360.))) -
     *  cos(l*(phi-(((2*3.14159265)*72.54)/360.))) -
     *  cos(l*(phi-(((2*3.14159265)*84.26)/360.))) -
     *  cos(l*(phi-(((2*3.14159265)*(180.-25.84))/360.)))-
     *  cos(l*(phi-(((2*3.14159265)*(180.-45.57))/360.)))-
     *  cos(l*(phi-(((2*3.14159265)*(180.-60.))/360.))) -
     *  cos(l*(phi-(((2*3.14159265)*(180.-72.54))/360.)))-
     *  cos(l*(phi-(((2*3.14159265)*(180.-84.26))/360.)))+
     *  cos(l*(phi-(((2*3.14159265)*(180.+25.84))/360.)))+
     *  cos(l*(phi-(((2*3.14159265)*(180.+45.57))/360.)))+
     *  cos(l*(phi-(((2*3.14159265)*(180.+60.))/360.))) +
     *  cos(l*(phi-(((2*3.14159265)*(180.+72.54))/360.)))+
     *  cos(l*(phi-(((2*3.14159265)*(180.+84.26))/360.)))+
     *  cos(l*(phi-(((2*3.14159265)*(360.-25.84))/360.)))+
     *  cos(l*(phi-(((2*3.14159265)*(360.-45.57))/360.)))+
     *  cos(l*(phi-(((2*3.14159265)*(360.-60.))/360.))) +
     *  cos(l*(phi-(((2*3.14159265)*(360.-72.54))/360.)))+
     *  cos(l*(phi-(((2*3.14159265)*(360.-84.26))/360.))))
        enddo

        Cu=Currnt*dR
        write(2,*) Cu , phi
        Cu=0.0

        do i=1,dim
         do j=1,dim
          d=(((dim-1)/2.)-i)-(b*cos(phi-
     *    ((2*3.14159265)/(2*n))))
          c=(((dim-1)/2.)-j)-(b*sin(phi-
     *    ((2*3.14159265)/(2*n))))
          r=sqrt((c**2)+(d**2))
          cosa=c/r
          sina=d/r
c         Write(*,*)d,c,' r=',r,' cosa=',cosa,sina

          Field(i,j,1)=Field(i,j,1)+(((1*Currnt*dR)/r)*cosa)
          Field(i,j,2)=Field(i,j,2)+(((1*Currnt*dR)/r)*sina)

           enddo
         enddo
         write(*,*)  'phi=',phi
c        ' i=',i,' j=',j,
        enddo

c Finished Calculating Field from shield


c Calculating Absolute Value of the Field

        do i=1,dim
         do j=1,dim
         AbsH(i,j)=sqrt((Field(i,j,1)**2)+(Field(i,j,2)**2))
         if(AbsH(i,j).gt.2.) AbsH(i,j)=2.0
         enddo
        enddo

c  Printout results for Field. Start
        do i=1,dim
           write(1,555)(AbsH(i,j),j=1,dim)
555        FORMAT(10000(1x,F20.15))
        enddo
c   Printout results for Field. Finished

        stop
        end
```

Appendix F

Coarsely -discretized current distribution

Listed below is the Fortran program used to calculate $|\vec{B}/\vec{B}_0|$ for a discrete (20 wire) sine-phi B_1 coil shielded by a coarsely-discretized (16 wire) current distribution. Once the variables a and b (the radii of inner and outer cylinders on which the currents flow) are defined, the program calculates the dimensionless ratio $|\vec{B_{tot}}(x,y)|/|\vec{B}_0|$ and stores the results in an array of size dim×dim (in this case 121×121). The central entry in the array (in this case 61,61) is associated with the coordinate ($x = 0$, $y = 0$). The program saves the array of $|\vec{B_{tot}}(x,y)|/|\vec{B}_0|$ values in the file "fort.1".

```
      real*8 Current, Field(1001,1001,2), AbsH(1001,1001)
      real*8 a,b,alfa,c,d,phi,r,cosa,sina,dR,Io,Currnt,Cu
      integer dim

c      Define parameters
      Io=1.
      dim=21
      a=5.4
c     50.*sqrt(4./5.)
      b=6.75
      n=360
      Current=0.0
      Currnt=0.0
      Cu=0.0

      do i=1,1001
       do j=1,1001
        Field(i,j,1)=0.
        Field(i,j,2)=0.
        AbsH(i,j)=0.
c       write(*,*)Field(i,j,1),Field(i,j,1), AbsH(i,j)
       enddo
      enddo
```

```
c Calculation of the field for 20 wires. Start
          do i=1,dim
            do j=1,dim

c  First quadrant Started
        d=(((dim-1)/2.)-i)-(a*cos((((2*3.14159265)
     *  *25.84)/360.)))
        c=(((dim-1)/2.)-j)-(a*sin((((2*3.14159265)
     *  *25.84)/360.)))
        r=sqrt((c**2)+(d**2))
        cosa=c/r
        sina=d/r
        Field(i,j,1)=Field(i,j,1)+((Io/r)*cosa)
        Field(i,j,2)=Field(i,j,2)+((Io/r)*sina)

        d=(((dim-1)/2.)-i)-(a*cos((((2*3.14159265)
     *  *45.57)/360.)))
        c=(((dim-1)/2.)-j)-(a*sin((((2*3.14159265)
     *  *45.57)/360.)))
        r=sqrt((c**2)+(d**2))
        cosa=c/r
        sina=d/r
c       Write(*,*)d,c,' r=',r,' cosa=',cosa,sina
        Field(i,j,1)=Field(i,j,1)+((Io/r)*cosa)
        Field(i,j,2)=Field(i,j,2)+((Io/r)*sina)

        d=(((dim-1)/2.)-i)-(a*cos((((2*3.14159265)
     *  *60.)/360.)))
        c=(((dim-1)/2.)-j)-(a*sin((((2*3.14159265)
     *  *60.)/360.)))
        r=sqrt((c**2)+(d**2))
        cosa=c/r
        sina=d/r
c       Write(*,*)d,c,' r=',r,' cosa=',cosa,sina

        Field(i,j,1)=Field(i,j,1)+((Io/r)*cosa)
        Field(i,j,2)=Field(i,j,2)+((Io/r)*sina)
        d=(((dim-1)/2.)-i)-(a*cos((((2*3.14159265)
     *  *72.54)/360.)))
        c=(((dim-1)/2.)-j)-(a*sin((((2*3.14159265)
     *  *72.54)/360.)))
        r=sqrt((c**2)+(d**2))
        cosa=c/r
        sina=d/r
c       Write(*,*)d,c,' r=',r,' cosa=',cosa,sina

        Field(i,j,1)=Field(i,j,1)+((Io/r)*cosa)
        Field(i,j,2)=Field(i,j,2)+((Io/r)*sina)
        d=(((dim-1)/2.)-i)-(a*cos((((2*3.14159265)
     *  *84.26)/360.)))
        c=(((dim-1)/2.)-j)-(a*sin((((2*3.14159265)
     *  *84.26)/360.)))
        r=sqrt((c**2)+(d**2))
        cosa=c/r
        sina=d/r
c       Write(*,*)d,c,' r=',r,' cosa=',cosa,sina
        Field(i,j,1)=Field(i,j,1)+((Io/r)*cosa)
        Field(i,j,2)=Field(i,j,2)+((Io/r)*sina)

c First Quadrant finished

c Second Quadrant Started

        d=(((dim-1)/2.)-i)-(a*cos((((2*3.14159265)
     *  *(180.-25.84))/360.)))
```

```
            c=(((dim-1)/2.)-j)-(a*sin((((2*3.14159265)
     *      *(180.-25.84))/360.)))
            r=sqrt((c**2)+(d**2))
            cosa=c/r
            sina=d/r
c           Write(*,*)d,c,' r=',r,' cosa=',cosa,sina
            Field(i,j,1)=Field(i,j,1)+((Io/r)*cosa)
            Field(i,j,2)=Field(i,j,2)+((Io/r)*sina)

            d=(((dim-1)/2.)-i)-(a*cos((((2*3.14159265)
     *      *(180.-45.57))/360.)))
            c=(((dim-1)/2.)-j)-(a*sin((((2*3.14159265)
     *      *(180.-45.57))/360.)))
            r=sqrt((c**2)+(d**2))
            cosa=c/r
            sina=d/r
c           Write(*,*)d,c,' r=',r,' cosa=',cosa,sina

            Field(i,j,1)=Field(i,j,1)+((Io/r)*cosa)
            Field(i,j,2)=Field(i,j,2)+((Io/r)*sina)


            d=(((dim-1)/2.)-i)-(a*cos((((2*3.14159265)
     *      *(180.-60.))/360.)))
            c=(((dim-1)/2.)-j)-(a*sin((((2*3.14159265)
     *      *(180.-60.))/360.)))
            r=sqrt((c**2)+(d**2))
            cosa=c/r
            sina=d/r
c           Write(*,*)d,c,' r=',r,' cosa=',cosa,sina

            Field(i,j,1)=Field(i,j,1)+((Io/r)*cosa)
            Field(i,j,2)=Field(i,j,2)+((Io/r)*sina)

            d=(((dim-1)/2.)-i)-(a*cos((((2*3.14159265)
     *      *(180.-72.54))/360.)))
            c=(((dim-1)/2.)-j)-(a*sin((((2*3.14159265)
     *      *(180.-72.54))/360.)))
            r=sqrt((c**2)+(d**2))
            cosa=c/r
            sina=d/r
c           Write(*,*)d,c,' r=',r,' cosa=',cosa,sina

            Field(i,j,1)=Field(i,j,1)+((Io/r)*cosa)
            Field(i,j,2)=Field(i,j,2)+((Io/r)*sina)

            d=(((dim-1)/2.)-i)-(a*cos((((2*3.14159265)
     *      *(180.-84.26))/360.)))
            c=(((dim-1)/2.)-j)-(a*sin((((2*3.14159265)
     *      *(180.-84.26))/360.)))
            r=sqrt((c**2)+(d**2))
            cosa=c/r
            sina=d/r
c           Write(*,*)d,c,' r=',r,' cosa=',cosa,sina

            Field(i,j,1)=Field(i,j,1)+((Io/r)*cosa)
            Field(i,j,2)=Field(i,j,2)+((Io/r)*sina)

c Second Quadrant finished

c Third Quadrant Started

            d=(((dim-1)/2.)-i)-(a*cos((((2*3.14159265)
     *      *(180.+25.84))/360.)))
            c=(((dim-1)/2.)-j)-(a*sin((((2*3.14159265)
     *      *(180.+25.84))/360.)))
```

```
        r=sqrt((c**2)+(d**2))
        cosa=c/r
        sina=d/r
c       Write(*,*)d,c,' r=',r,' cosa=',cosa,sina
        Field(i,j,1)=Field(i,j,1)+(((-1.*Io)/r)*cosa)
        Field(i,j,2)=Field(i,j,2)+(((-1.*Io)/r)*sina)

        d=(((dim-1)/2.)-i)-(a*cos((((2*3.14159265)
     *  *(180.+45.57))/360.)))
        c=(((dim-1)/2.)-j)-(a*sin((((2*3.14159265)*(180.+45.57))/360.)))
        r=sqrt((c**2)+(d**2))
        cosa=c/r
        sina=d/r
c       Write(*,*)d,c,' r=',r,' cosa=',cosa,sina

        Field(i,j,1)=Field(i,j,1)+(((-1.*Io)/r)*cosa)
        Field(i,j,2)=Field(i,j,2)+(((-1.*Io)/r)*sina)

        d=(((dim-1)/2.)-i)-(a*cos((((2*3.14159265)
     *  *(180.+60.))/360.)))
        c=(((dim-1)/2.)-j)-(a*sin((((2*3.14159265)
     *  *(180.+60.))/360.)))
        r=sqrt((c**2)+(d**2))
        cosa=c/r
        sina=d/r
c       Write(*,*)d,c,' r=',r,' cosa=',cosa,sina

        Field(i,j,1)=Field(i,j,1)+(((-1.*Io)/r)*cosa)
        Field(i,j,2)=Field(i,j,2)+(((-1.*Io)/r)*sina)

        d=(((dim-1)/2.)-i)-(a*cos((((2*3.14159265)
     *  *(180.+72.54))/360.)))
        c=(((dim-1)/2.)-j)-(a*sin((((2*3.14159265)
     *  *(180.+72.54))/360.)))
        r=sqrt((c**2)+(d**2))
        cosa=c/r
        sina=d/r
c       Write(*,*)d,c,' r=',r,' cosa=',cosa,sina

        Field(i,j,1)=Field(i,j,1)+(((-1.*Io)/r)*cosa)
        Field(i,j,2)=Field(i,j,2)+(((-1.*Io)/r)*sina)

        d=(((dim-1)/2.)-i)-(a*cos((((2*3.14159265)
     *  *(180.+84.26))/360.)))
        c=(((dim-1)/2.)-j)-(a*sin((((2*3.14159265)
     *  *(180.+84.26))/360.)))
        r=sqrt((c**2)+(d**2))
        cosa=c/r
        sina=d/r
c       Write(*,*)d,c,' r=',r,' cosa=',cosa,sina

        Field(i,j,1)=Field(i,j,1)+(((-1.*Io)/r)*cosa)
        Field(i,j,2)=Field(i,j,2)+(((-1.*Io)/r)*sina)

c Third Quadrant Finished

c Fourth Quadrant Started

        d=(((dim-1)/2.)-i)-(a*cos((((2*3.14159265)
     *  *(360.-25.84))/360.)))
        c=(((dim-1)/2.)-j)-(a*sin((((2*3.14159265)
     *  *(360.-25.84))/360.)))
        r=sqrt((c**2)+(d**2))
        cosa=c/r
        sina=d/r
c       Write(*,*)d,c,' r=',r,' cosa=',cosa,sina
```

```
        Field(i,j,1)=Field(i,j,1)+(((-1.*Io)/r)*cosa)
        Field(i,j,2)=Field(i,j,2)+(((-1.*Io)/r)*sina)


        d=(((dim-1)/2.)-i)-(a*cos((((2*3.14159265)
     *  *(360.-45.57))/360.)))
        c=(((dim-1)/2.)-j)-(a*sin((((2*3.14159265)
     *  *(360.-45.57))/360.)))
        r=sqrt((c**2)+(d**2))
        cosa=c/r
        sina=d/r
c       Write(*,*)d,c,' r=',r,' cosa=',cosa,sina

        Field(i,j,1)=Field(i,j,1)+(((-1.*Io)/r)*cosa)
        Field(i,j,2)=Field(i,j,2)+(((-1.*Io)/r)*sina)

        d=(((dim-1)/2.)-i)-(a*cos((((2*3.14159265)
     *  *(360.-60.))/360.)))
        c=(((dim-1)/2.)-j)-(a*sin((((2*3.14159265)
     *  *(360.-60.))/360.)))
        r=sqrt((c**2)+(d**2))
        cosa=c/r
        sina=d/r
c       Write(*,*)d,c,' r=',r,' cosa=',cosa,sina

        Field(i,j,1)=Field(i,j,1)+(((-1.*Io)/r)*cosa)
        Field(i,j,2)=Field(i,j,2)+(((-1.*Io)/r)*sina)

        d=(((dim-1)/2.)-i)-(a*cos((((2*3.14159265)
     *  *(360.-72.54))/360.)))
        c=(((dim-1)/2.)-j)-(a*sin((((2*3.14159265)
     *  *(360.-72.54))/360.)))
        r=sqrt((c**2)+(d**2))
        cosa=c/r
        sina=d/r
c       Write(*,*)d,c,' r=',r,' cosa=',cosa,sina

        Field(i,j,1)=Field(i,j,1)+(((-1.*Io)/r)*cosa)
        Field(i,j,2)=Field(i,j,2)+(((-1.*Io)/r)*sina)

        d=(((dim-1)/2.)-i)-(a*cos((((2*3.14159265)
     *  *(360.-84.26))/360.)))
        c=(((dim-1)/2.)-j)-(a*sin((((2*3.14159265)
     *  *(360.-84.26))/360.)))
        r=sqrt((c**2)+(d**2))
        cosa=c/r
        sina=d/r
c       Write(*,*)d,c,' r=',r,' cosa=',cosa,sina

        Field(i,j,1)=Field(i,j,1)+(((-1.*Io)/r)*cosa)
        Field(i,j,2)=Field(i,j,2)+(((-1.*Io)/r)*sina)

c Fourth Quadrant Finished

c Calculate Field from shield --- 16 wires
c  Shield First quadrant Started

        d=(((dim-1)/2.)-i)-(b*cos((((2*3.14159265)
     *  *28.)/360.)))
        c=(((dim-1)/2.)-j)-(b*sin((((2*3.14159265)
     *  *28.)/360.)))
        r=sqrt((c**2)+(d**2))
        cosa=c/r
        sina=d/r
```

```
            Field(i,j,1)=Field(i,j,1)+((-1.*Io/r)*cosa)
            Field(i,j,2)=Field(i,j,2)+((-1.*Io/r)*sina)

            d=(((dim-1)/2.)-i)-(b*cos((((2*3.14159265)
     *      *51.)/360.)))
            c=(((dim-1)/2.)-j)-(b*sin((((2*3.14159265)
     *      *51.)/360.)))
            r=sqrt((c**2)+(d**2))
            cosa=c/r
            sina=d/r
c           Write(*,*)d,c,' r=',r,' cosa=',cosa,sina

            Field(i,j,1)=Field(i,j,1)+((-1.*Io/r)*cosa)
            Field(i,j,2)=Field(i,j,2)+((-1.*Io/r)*sina)

            d=(((dim-1)/2.)-i)-(b*cos((((2*3.14159265)
     *      *68.)/360.)))
            c=(((dim-1)/2.)-j)-(b*sin((((2*3.14159265)
     *      *68.)/360.)))
            r=sqrt((c**2)+(d**2))
            cosa=c/r
            sina=d/r
c           Write(*,*)d,c,' r=',r,' cosa=',cosa,sina

            Field(i,j,1)=Field(i,j,1)+((-1.*Io/r)*cosa)
            Field(i,j,2)=Field(i,j,2)+((-1.*Io/r)*sina)

            d=(((dim-1)/2.)-i)-(b*cos((((2*3.14159265)
     *      *83.)/360.)))
            c=(((dim-1)/2.)-j)-(b*sin((((2*3.14159265)
     *      *83.)/360.)))
            r=sqrt((c**2)+(d**2))
            cosa=c/r
            sina=d/r
c           Write(*,*)d,c,' r=',r,' cosa=',cosa,sina

            Field(i,j,1)=Field(i,j,1)+((-1.*Io/r)*cosa)
            Field(i,j,2)=Field(i,j,2)+((-1.*Io/r)*sina)

c Shield First Quadrant finished

c Shield Second Quadrant Started

            d=(((dim-1)/2.)-i)-(b*cos((((2*3.14159265)
     *      *(180.-28.))/360.)))
            c=(((dim-1)/2.)-j)-(b*sin((((2*3.14159265)
     *      *(180.-28.))/360.)))
            r=sqrt((c**2)+(d**2))
            cosa=c/r
            sina=d/r
c           Write(*,*)d,c,' r=',r,' cosa=',cosa,sina

            Field(i,j,1)=Field(i,j,1)+((-1.*Io/r)*cosa)
            Field(i,j,2)=Field(i,j,2)+((-1.*Io/r)*sina)

            d=(((dim-1)/2.)-i)-(b*cos((((2*3.14159265)
     *      *(180.-51.))/360.)))
            c=(((dim-1)/2.)-j)-(b*sin((((2*3.14159265)
     *      *(180.-51.))/360.)))
            r=sqrt((c**2)+(d**2))
            cosa=c/r
            sina=d/r
c           Write(*,*)d,c,' r=',r,' cosa=',cosa,sina

            Field(i,j,1)=Field(i,j,1)+((-1.*Io/r)*cosa)
            Field(i,j,2)=Field(i,j,2)+((-1.*Io/r)*sina)
```

```
        d=(((dim-1)/2.)-i)-(b*cos((((2*3.14159265)
     *  *(180.-68.))/360.)))
        c=(((dim-1)/2.)-j)-(b*sin((((2*3.14159265)
     *  *(180.-68.))/360.)))
        r=sqrt((c**2)+(d**2))
        cosa=c/r
        sina=d/r
c       Write(*,*)d,c,' r=',r,' cosa=',cosa,sina

        Field(i,j,1)=Field(i,j,1)+((-1.*Io/r)*cosa)
        Field(i,j,2)=Field(i,j,2)+((-1.*Io/r)*sina)

        d=(((dim-1)/2.)-i)-(b*cos((((2*3.14159265)
     *  *(180.-83.))/360.)))
        c=(((dim-1)/2.)-j)-(b*sin((((2*3.14159265)
     *  *(180.-83.))/360.)))
        r=sqrt((c**2)+(d**2))
        cosa=c/r
        sina=d/r
c       Write(*,*)d,c,' r=',r,' cosa=',cosa,sina

        Field(i,j,1)=Field(i,j,1)+((-1.*Io/r)*cosa)
        Field(i,j,2)=Field(i,j,2)+((-1.*Io/r)*sina)

c Shield Second Quadrant finished

c Shield Third Quadrant Started

        d=(((dim-1)/2.)-i)-(b*cos((((2*3.14159265)
     *  *(180.+28.))/360.)))
        c=(((dim-1)/2.)-j)-(b*sin((((2*3.14159265)
     *  *(180.+28.))/360.)))
        r=sqrt((c**2)+(d**2))
        cosa=c/r
        sina=d/r
c       Write(*,*)d,c,' r=',r,' cosa=',cosa,sina

        Field(i,j,1)=Field(i,j,1)+(((Io)/r)*cosa)
        Field(i,j,2)=Field(i,j,2)+(((Io)/r)*sina)

        d=(((dim-1)/2.)-i)-(b*cos((((2*3.14159265)
     *  *(180.+51.))/360.)))
        c=(((dim-1)/2.)-j)-(b*sin((((2*3.14159265)
     *  *(180.+51.))/360.)))
        r=sqrt((c**2)+(d**2))
        cosa=c/r
        sina=d/r
c       Write(*,*)d,c,' r=',r,' cosa=',cosa,sina

        Field(i,j,1)=Field(i,j,1)+(((Io)/r)*cosa)
        Field(i,j,2)=Field(i,j,2)+(((Io)/r)*sina)

        d=(((dim-1)/2.)-i)-(b*cos((((2*3.14159265)
     *  *(180.+68.))/360.)))
        c=(((dim-1)/2.)-j)-(b*sin((((2*3.14159265)
     *  *(180.+68.))/360.)))
        r=sqrt((c**2)+(d**2))
        cosa=c/r
        sina=d/r
c       Write(*,*)d,c,' r=',r,' cosa=',cosa,sina

        Field(i,j,1)=Field(i,j,1)+(((Io)/r)*cosa)
        Field(i,j,2)=Field(i,j,2)+(((Io)/r)*sina)

        d=(((dim-1)/2.)-i)-(b*cos((((2*3.14159265)
```

```
     *  *(180.+83.))/360.)))
        c=(((dim-1)/2.)-j)-(b*sin((((2*3.14159265)
     *  *(180.+83.))/360.)))
        r=sqrt((c**2)+(d**2))
        cosa=c/r
        sina=d/r
c       Write(*,*)d,c,' r=',r,' cosa=',cosa,sina

        Field(i,j,1)=Field(i,j,1)+(((Io)/r)*cosa)
        Field(i,j,2)=Field(i,j,2)+(((Io)/r)*sina)

c Shield Third Quadrant Finished

c Shield Fourth Quadrant Started

        d=(((dim-1)/2.)-i)-(b*cos((((2*3.14159265)
     *  *(360.-28.))/360.)))
        c=(((dim-1)/2.)-j)-(b*sin((((2*3.14159265)
     *  *(360.-28.))/360.)))
        r=sqrt((c**2)+(d**2))
        cosa=c/r
        sina=d/r
c       Write(*,*)d,c,' r=',r,' cosa=',cosa,sina

        Field(i,j,1)=Field(i,j,1)+(((Io)/r)*cosa)
        Field(i,j,2)=Field(i,j,2)+(((Io)/r)*sina)

        d=(((dim-1)/2.)-i)-(b*cos((((2*3.14159265)
     *  *(360.-51.))/360.)))
        c=(((dim-1)/2.)-j)-(b*sin((((2*3.14159265)
     *  *(360.-51.))/360.)))
        r=sqrt((c**2)+(d**2))
        cosa=c/r
        sina=d/r
c       Write(*,*)d,c,' r=',r,' cosa=',cosa,sina

        Field(i,j,1)=Field(i,j,1)+(((Io)/r)*cosa)
        Field(i,j,2)=Field(i,j,2)+(((Io)/r)*sina)

        d=(((dim-1)/2.)-i)-(b*cos((((2*3.14159265)
     *  *(360.-68.))/360.)))
        c=(((dim-1)/2.)-j)-(b*sin((((2*3.14159265)
     *  *(360.-68.))/360.)))
        r=sqrt((c**2)+(d**2))
        cosa=c/r
        sina=d/r
c       Write(*,*)d,c,' r=',r,' cosa=',cosa,sina

        Field(i,j,1)=Field(i,j,1)+(((Io)/r)*cosa)
        Field(i,j,2)=Field(i,j,2)+(((Io)/r)*sina)

        d=(((dim-1)/2.)-i)-(b*cos((((2*3.14159265)
     *  *(360.-83.))/360.)))
        c=(((dim-1)/2.)-j)-(b*sin((((2*3.14159265)
     *  *(360.-83.))/360.)))
        r=sqrt((c**2)+(d**2))
        cosa=c/r
        sina=d/r
c       Write(*,*)d,c,' r=',r,' cosa=',cosa,sina

        Field(i,j,1)=Field(i,j,1)+(((Io)/r)*cosa)
        Field(i,j,2)=Field(i,j,2)+(((Io)/r)*sina)

c Shield Fourth Quadrant Finished

c Finished Calculate Field from shield finished 16 wires
```

```
          enddo
         enddo

c Calculating Absolute Value of the Field

        do i=1,dim
          do j=1,dim
           AbsH(i,j)=sqrt((Field(i,j,1)**2)+(Field(i,j,2)**2))
           if(AbsH(i,j).gt.1.2) AbsH(i,j)=1.2
          enddo
        enddo

c FINISHED Calculating Absolute Value of the Field

c  Printout results for Field. Start
        do i=1,dim
           write(1,555)(AbsH(i,j),j=1,dim)
555        FORMAT(10000(1x,F20.15))
        enddo
c   Printout results for Field. Finished

        stop
        end
```

Bibliography

[1] I.B. Khrilpovich and S.K. Lamoreaux, *CP Violation Without Strangeness*, chapter 3, p. 41, (Springer-Verlag Berlin Heidelberg ,1997).

[2] C.P. Bidinosti, I.S. Kravchuk and M.E. Hayden, Active Shielding of Cylindrical Saddle-shaped Coils: Application to Wire-wound RF Coils for Very Low Field NMR and MRI, J. of Magn. Reson. (in press).

[3] M.S. Albert *et al.*, Nature 370, 199 (1994)

[4] C.E. Hayes, W.A. Edelstein, and J.F. Schneck, Radio Frequency Resonators, chapter 72, pp. 1183 - 1200 in *Magnetic Resonance Imaging*, 2nd ed. (W.B. Saunders, Philadelphia, 1988).

[5] J.A. Tegopoulos *et al.*, Eddy Currents in Cylindrical Shells Due to Parallel Conductors, chapter 6, pp. 112 - 1125 in *Eddy Currents in Linear Conducting Media*, (Elsevier, Amsterdam, 1985).

[6] J.-M. Jin, Electromagnetics in magnetic resonance imaging, IEEE Antennas and Propagation Magazine 40 (1998) 7 - 22.

[7] S. Fahy, Charles Kittel, and Steven G. Lovie, Electromagnetic Screening by Metals, Am. J. Phys. 56 (1988) 989 - 992.

[8] P. Mansfield and B. Chapman, Active magnetic screening of coils for static and time-dependent magnetic field generation in NMR imaging, J. Phys. E: Sci. Instrum. 19 (1986) 540 - 545.

[9] R. Turner and R.M. Bowley, Passive screening of switched magnetic field gradients, J. Phys. E: Sci. Instrum. 19 (1986) 876 - 879.

[10] R. Turner, Gradient coil design - a review of methods, Magn. Reson. Imaging 11 (1993) 903 - 920.

[11] D.O. Kuethe *et al.*, J. Appl. Physiol., 88:2279-86 (2000)

[12] F. Kober *et al.*, J. Magn. Reson., 138:308-12 (1999)

[13] W.R. Abel, A.C. Anderson, W.C. Black, and J.C. Wheatley, Thermal and magnetic properties of liquid He^3 at low pressure and very low temperatures, Physica 1 (1965) 337 - 387. (See Section III. D. 2. as well as Footnote 58 in the References section of this paper. The pertinent details of these sections are also summarized in [14].)

[14] D.M. Ginsberg and M.J. Melchner, Optimum geometry of saddle shaped coils for generating a uniform magnetic field, Rev. Sci. Instrum. 41 (1970) 122 - 123.

[15] D.I. Hoult and R.E. Richards, The signal-to-noise ratio of the nuclear magnetic resonance experiment, J. Magn. Reson. 24 (1976) 71 - 85.

[16] D.I. Hoult, The NMR receiver: A description and analysis of design, Progress in NMR Spectroscopy 12 (1978) 41 - 77.

[17] F. Roméo and D.I. Hoult, Magnet Field Profiling: Analysis and Correcting Coil Design, Magn. Reson. Med. 1 (1984) 44 - 65.

[18] H. Hanssum, Exact Solution of the Poisson Equation for a DC Current on a Saddle-Shaped Helmholtz Coil, J. Phys. A: Math. Gen. 16 (1983) 3385 - 3392.

[19] H. Hanssum, The magnetic field of saddle-shaped coils: I. Symmetry of the magnetic field around the coil centre, J. Phys. D: Appl. Phys. 17 (1984) 1 - 18.

[20] H. Hanssum, The magnetic field of saddle-shaped coils: II. Transverse components, J. Phys. D: Appl. Phys. 18 (1985) 1971 - 1978.

[21] H. Hanssum, The magnetic field of saddle-shaped coils: III. Improving the uniformity of $|B|$ in a large volume, J. Phys. D: Appl. Phys. 19 (1986) 493 - 501.

[22] J.D. Jackson, *Classical Electrodynamics*, 3rd ed. (Wiley, New York, 1999).

[23] M. Abramowitz and I.A. Stegun, *Handbook of Mathematical Functions*, 9th printing (Dover, New York, 1970).

[24] *Stanford Research System Model SR830 DSP Lock-in Amplifier Manual, Revision 1.6*, Stanford Research Systems, Sunnyvale CA, Sept.2000 Ch.3 SR830 BASICS.

[25] D. Budker, A. Sushkov, V. Yaskchuk, B. Filippone, T. Ito, R. McKeown, R. Golub, K. Korobkina, J. Doyle, D. Beck, D. Hertzog, P. Kammel, J.-C. Peng, S. Williamson, J. Butterworth, G. Frossati, P. Barnes, J. Boissevain, M. Cooper, M. Espy, S. Lamoreaux, A. Matlachov, R. Mischke, S. Penttila, J. Torgerson, E. Beise, H. Breuer, P. Ross, D. Dutta, H. Gao, T. Gentile, P. Huffman, A. Babkin, R. Dunkan, V. Cianciolo, and M.E. Hayden, *A New Search for the Electric Dipole Moment of the Neutron*, funding pre-proposal submitted to the US Department of Energy (March 28, 2002). Also available online at http://p25ext.lanl.gov/edm/ pdf.unprotected/ EDM_proposal.pdf